

Research Article

The Sydney Radio Star Catalogue: Properties of radio stars at megahertz to gigahertz frequencies

Laura Nicole Driessen¹, Joshua Pritchard¹, Tara Murphy¹, George Heald², Jan Robrade³, Barnali Das², Stefan William Duchesne², David L. Kaplan⁴, Emil Lenc⁵, Christene R. Lynch⁶, Jackson Mitchell-Bolton¹, Benjamin J.S. Pope^{7,8}, Kovi Rose^{1,5}, Beate Stelzer⁹, Yuanming Wang¹⁰ and Andrew Zic⁵

¹Sydney Institute for Astronomy, School of Physics, The University of Sydney, Sydney, NSW, Australia, ²Australian Telescope National Facility, CSIRO, Space and Astronomy, Bentley, WA, Australia, ³Hamburger Sternwarte, Universität Hamburg, Hamburg, Germany, ⁴Center for Gravitation, Cosmology, and Astrophysics, Department of Physics, University of Wisconsin-Milwaukee, Milwaukee, WI, USA, ⁵Australian Telescope National Facility, CSIRO Astronomy and Space Science, Epping, NSW, Australia, ⁶Department of Physics and Astronomy, University of North Carolina Asheville, Asheville, NC, USA, ⁷School of Mathematics and Physics, University of Queensland, St Lucia, QLD, Australia, ⁸Centre for Astrophysics, University of Southern Queensland, Toowoomba, QLD, Australia, ⁹Institut für Astronomie und Astrophysik, Eberhard Karls Universität Tübingen, Tübingen, Germany and ¹⁰Centre for Astrophysics and Supercomputing, Swinburne University of Technology, Hawthorn, VIC, Australia

Abstract

We present the Sydney Radio Star Catalogue, a new catalogue of stars detected at megahertz to gigahertz radio frequencies. It consists of 839 unique stars with 3 405 radio detections, more than doubling the previously known number of radio stars. We have included stars from large area searches for radio stars found using circular polarisation searches, cross-matching, variability searches, and proper motion searches as well as presenting hundreds of newly detected stars from our search of Australian SKA Pathfinder observations. The focus of this first version of the catalogue is on objects detected in surveys using SKA precursor and pathfinder instruments; however, we will expand this scope in future versions. The 839 objects in the Sydney Radio Star Catalogue are distributed across the whole sky and range from ultracool dwarfs to Wolf-Rayet stars. We demonstrate that the radio luminosities of cool dwarfs are lower than the radio luminosities of more evolved sub-giant and giant stars. We use X-ray detections of 530 radio stars by the eROSITA soft X-ray instrument onboard the Spectrum Roentgen Gamma spacecraft to show that almost all of the radio stars in the catalogue are over-luminous in the radio, indicating that the majority of stars at these radio frequencies are coherent radio emitters. The Sydney Radio Star Catalogue can be found in Vizier or at https://radiostars.org.

Keywords: Radio continuum: stars; stars: flare; stars: variables: general; X-rays: stars; stars: Wolf-Rayet

(Received 11 April 2024; revised 10 July 2024; accepted 13 August 2024)

1. Introduction

Radio emission has been detected from stars across the main sequence and beyond (e.g. Matthews 2019), from ultracool dwarfs (UCDs, e.g. Berger et al. 2001; Route & Wolszczan 2012; Williams & Berger 2015; Kao et al. 2018) to Wolf-Rayet stars (e.g. Seaquist 1976; Abbott et al. 1986; Dougherty et al. 2005). Radio emission provides information about the coronae and magnetic fields of stars (Dulk 1985; Güdel 2002; Matthews 2019) and has the potential to reveal magnetic interaction between stars and planets (e.g. Vedantham et al. 2020; Shiohira et al. 2024). Radio observations and multi-wavelength studies of stars have been used to investigate a range of stellar phenomena and physics. This includes constraining and investigating stellar coronal mass ejections and transient mass loss (e.g. Crosley & Osten 2018; Zic et al. 2020) and magnetic dissipation via winds (Vidotto et al. 2012). Radio observations

Corresponding author: Laura Nicole Driessen; Email: Laura.Driessen@sydney.edu.au Cite this article: Driessen LN, Pritchard J, Murphy T, Heald G, Robrade J, Das B, Duchesne SW, Kaplan DL, Lenc E, Lynch CR, Mitchell-Bolton J, Pope BJS, Rose K, Stelzer B, Wang Y and Zic A. (2024) The Sydney Radio Star Catalogue: Properties of radio stars at megahertz to gigahertz frequencies. *Publications of the Astronomical Society of Australia* 41, e084, 1–18. https://doi.org/10.1017/pasa.2024.72

have also shed light on stellar dynamo models (Kao et al. 2016), magnetospheric topology (e.g. Berger et al. 2009; Lynch, Mutel, & Güdel 2015; Bastian, Cotton, & Hallinan 2022), UCD radiation belts (Kao et al. 2023; Climent et al. 2023), magnetospheric density structures in hot stars (Das, Chandra, & Wade 2020), and magnetic interactions in binary systems (Biswas et al. 2023). Radio stars are a useful tool for linking the optical and radio coordinate reference frames (e.g. Walter, Hering, & de Vegt 1997) and and are likely to be one of the most common variable objects detected by the Square Kilometre Array after Active Galactic Nuclei (AGN). It is therefore important to identify and study a larger population of radio stars.

The first stars to be detected at radio frequencies were identified in 1963 (Lovell, Whipple, & Solomon 1963; Slee 1963), four years before the discovery of the first pulsar (Hewish et al. 1968). Despite this, the number of known radio stars has remained low, with one of the key challenges in identifying them being chance coincidence between stars and radio galaxies (Callingham et al. 2019b). The canonical catalogue for radio stars is the Catalogue of Radio Stars (CRS;Wendker 1978, 1987, 1995), which was last updated on 2001 March 26. It contains 228 radio stars detected at <3 GHz. The CRS has been an excellent resource; however, recent

© The Author(s), 2024. Published by Cambridge University Press on behalf of Astronomical Society of Australia. This is an Open Access article, distributed under the terms of the Creative Commons Attribution licence (https://creativecommons.org/licenses/by/4.0/), which permits unrestricted re-use, distribution and reproduction, provided the original article is properly cited.

wide-area radio surveys at <3 GHz, and new radio star identifications, mean that it no longer reflects the population of known radio stars, and a comprehensive update is needed.

Recently, large sky area surveys with the Australian SKA Pathfinder (ASKAP;^a Hotan et al. 2021) and the Low Frequency Array (LOFAR; van Haarlem et al. 2013) have significantly increased the number of known radio emitting stars by using circular polarisation (Stokes V), variability, and proper motion searches. One reason for this success is that high circular polarisation fraction (>10%) can be used to exclude AGN, the dominant type of radio point source by far, since radio-bright AGN have a circular polarisation fraction ≤1% (e.g. Saikia & Salter 1988; O'Sullivan et al. 2013). Using this method with the LOFAR telescope, Callingham et al. (2021) and Toet et al. (2021) identified 18 previously unknown radio-active M stars and detected one known radio-active M star and 14 known radio-active RS Canum Venaticorum (RS CVn) binaries. The M dwarfs reported by Callingham et al. (2021) and RS CVns reported by Toet et al. (2021) were included in the LOFAR Two-metre Sky Survey (LoTSS; Shimwell et al. 2017, 2022) in Stokes V (V-LoTSS Callingham et al. 2023) paper as well as some new radio star identifications for a total of 37 radio identified stars. Pritchard et al. (2021) used ASKAP Stokes V detections to identify 23 previously unknown radio stars and 10 known ones. Pritchard et al. (2024) expanded on this work and found 36 radio stars by performing multi-epoch Stokes V searches using ASKAP.

Untargeted searches for variable radio sources have resulted in detections of flares from eight stars using ASKAP (Wang et al. 2023) and three stars (Driessen et al. 2020, 2022; Andersson et al. 2022) using the (more) Karoo Array Telescope (MeerKAT; Camilo et al. 2018). Driessen et al. (2023) identified eight radio stars, two of which had not previously been identified, by searching for changes in radio position due to proper motion.

Cross-matching directly between radio point source surveys and optical sky surveys such as Gaia (Gaia Collaboration et al. 2016b, 2023; Babusiaux et al. 2023) results in a high chance coincidence rate (Callingham et al. 2019b) between radio AGN and optical stars. However, the probability of chance coincidence decreases when limited samples are used, such as volume-limited samples. For example, cross-matching between the Karl G. Jansky Very Large Array (VLA; Perley et al. 2011) Faint Images of the Radio Sky at Twenty centimetres (FIRST; Becker, White, & Helfand 1994, 1995) survey and various optical catalogues resulted in the detection of 26 radio stars (Helfand et al. 1999). They calculated that 0.96 ± 0.04 of their matches with Hipparcos (Perryman et al. 1997) were by chance. At the time, this doubled the number of known radio stars in the area of sky covered by the search. This was a cross-match using a comparatively limited sample as FIRST contains 946 000 sources over 10 000 square degrees (~90 sources per square degree) while the Hipparcos catalogue contains 118 218 sources over the whole sky (3 sources per square degree). This is compared to LoTSS, for example, which contains 4 396 228 radio sources over 5 635 square degrees (780 sources per square degree) and the Gaia DR3 catalogue which contains 1.46 billion sources over the whole sky (\sim 35 000 sources per square degree). Yiu et al. (2024) successfully cross-matched the radio surveys LoTSS and the VLA Sky Survey (VLASS; Lacy et al. 2020; Gordon et al. 2021) with the Gaia catalogue of Nearby Stars (GCNS; Gaia Collaboration et al. 2021b). They found 25 LoTSS-GCNS radio stars with an

estimated number of chance coincidence matches of \sim 1 and 65 VLASS-GCNS radio stars with an estimated number of chance coincidence matches of \sim 0.5. This shows that we can improve reliability by either cross-matching to a volume-limited stellar sample or by cross-matching the radio source catalogue to a subset of stars.

In this paper, we present a new catalogue of 839 unique radio stars: the Sydney Radio Star Catalogue (SRSC). This includes hundreds of new radio star identifications found by performing circular polarisation and cross-match searches using ASKAP. We focus on producing a reliable catalogue using only stars from large-scale, wide-field searches for radio stars using SKA precursor and pathfinder instruments. We aim to provide a useful resource for the radio star community, and we plan to update the web version of the catalogue to include published radio stars and future radio star identifications. In Section 2, we present the catalogues and search methods used to identify the radio stars included in the SRSC. In Section 3, we present the format of the catalogue. In Section 4, we present the content and properties of the SRSC. We summarise in Section 5.

2. Radio star identification methods

The catalogue is constructed from samples of confirmed radio stars already published in the literature, as well as newly detected radio stars from the work presented here. We have only included stars from searches for radio stars using SKA precursors and pathfinders for which the detection of radio emission is confirmed and reliable. We have not included candidate radio stars, for which the association is not confirmed.

In this section, we will present the method for and results of searching for new radio star identifications using ASKAP via circular polarisation searches (Section 2.1) and cross-matching (Section 2.2). We will also detail what other samples of stars are included in the SRSC (Section 2.3) and those that we have chosen not to include for this version of the SRSC (Section 2.4).

2.1. ASKAP circular polarisation searches

We include 235 stars discovered via circular polarisation searches of Rapid ASKAP Continuum Survey (RACS) data and Variables and Slow Transients with ASKAP (VAST; Murphy et al. 2013) Pilot (VASTP) survey data. RACS is the ASKAP all-sky radio survey and has been conducted at three frequencies: 887.5 MHz (RACS-low; McConnell et al. 2020; Hale et al. 2021), 1 367.5MHz (RACS-mid; Duchesne et al. 2023), and at 1 655.5 MHz (RACS-high; Duchesne et al. in preparation). RACS-low covers the southern sky up to +40° declination and both RACS-mid and RACS-high cover the southern sky up to +50° declination. RACS-low, RACS-mid, and RACS-high are currently available in the CSIRO ASKAP Science Data Archive (CASDA). The initial RACS-high release will be further processed and combined into an individual catalogue as part of a future publication (Duchesne et al. in preparation).

The VAST team is performing untargeted searches for variable and transient radio sources in 12-min, 887.5 MHz ASKAP observations. VASTP-low is the low band of the VAST pilot survey at 887.5 MHz which covered a 5 131 deg² footprint with a varying degree of coverage over 15 epochs (see Murphy et al. 2021 and Pritchard et al. 2024 for details). The circular polarisation search

^ahttps://www.atnf.csiro.au/projects/askap/index.html.

bhttps://research.csiro.au/casda/https://research.csiro.au/casda/.

presented here used RACS-low, RACS-mid, and RACS-high data as well as the VASTP data. We refer the reader to Pritchard et al. (2021) and (2024) for a detailed discussion of the circular polarisation search method, artefact rejection, and classification procedure, and summarise the main points here. In each search the SELAVY (Whiting 2012; Whiting & Humphreys 2012) source finder package was used to extract lists of 2D Gaussian source components from the Stokes I and V images, and sources with significant circular polarisation were identified by crossmatching the extracted Stokes V components with their counterparts in Stokes I. The candidates were restricted to Stokes I-V associations that were greater than 5σ in both Stokes I and V where σ is the local RMS noise, and with fractional circular polarisation $|S_V|/S_I > 6\%$, corresponding to 10 times the median polarisation leakage of Stokes I into V (Pritchard et al. 2024).

After manual rejection of Stokes I-V associations with artificially high $|S_V|/S_I$ caused by imaging artefacts and noise, 47 radio stars were identified in RACS-low, 65 radio stars in RACS-mid, 64 radio stars in RACS-high and 184 detections of 36 stars over the multi-epoch VASTP-low survey. The detection rate of stars detected via circular polarisation searches of 15 epochs of VASTP low has been explored in Pritchard et al. (2024). The majority of late-type dwarfs show a high degree of variability and detection rates of <10%, while interacting binary systems are persistently detected. Declinations below $+40^\circ$ are covered by all three RACS (low, mid, and high) surveys. In this sky area there are 47 RACS-low, 63 RACS-mid, and 59 RACS-high stars found via circular polarisation searches. Of these stars:

- 7 were found in both RACS-low and RACS-mid
- 3 were found in both RACS-low and RACS-high
- 4 were found in both RACS-mid and RACS-high
- 1 was found in RACS-low, RACS-mid and RACS-high.

Similar to the investigation by Pritchard et al. (2024), the low number of repeat detections in the RACS surveys indicates that variability has a significant impact on radio detections of circularly polarised stars.

2.2 ASKAP catalogue cross-matching

We used cross-matching between ASKAP radio point source positions and selected star catalogues to search for radio stars. We reduced the chance-coincidence probability of the cross-matches by using star catalogues that were either volume limited, or only included a subset of stars. This approach resulted in the identification of 734 stars. In this section, we describe this method, the ASKAP and star catalogues we used for cross-matching, and our results.

2.2.1 ASKAP sample preparation

We used all publicly available ASKAP data in CASDA as of 2023 October 16, as well as RACS-low, RACS-mid, and RACS-high data. The ASKAP data available in CASDA varies in integration time and frequency. The integration times range from just under a minute to thirteen hours. The observations have frequency

^cRACS-high was searched to $|S_V|/S_I > 6\%$ within 3.75° of the field centre, and $|S_V|/S_I > 10\%$ outside this range where leakage increases towards the field edges (Pritchard et al. 2024).

Table 1. Number of sources, $N_{\rm ASKAP}$, in each ASKAP samples. $N_{\rm ASKAP}$ is the total number of ASKAP sources in each catalogue, excluding duplicate sources. $N_{\rm ASKAP,IG}$ is the number of ASKAP sources in each catalogue after the Milliquas and 6dFGSzDR3 cross-matched sources have been removed. $N_{\rm ASKAP,IG,PS}$ is the number of ASKAP sources in each catalogue after the Milliquas and 6dFGSzDR3 cross-matched sources have been removed and after removing sources where $S_{\rm int}/S_{\rm peak} > 1.5$.

| Sample name | N _{ASKAP} | N _{ASKAP,!G} | N _{ASKAP,!G,PS} |
|-------------|--------------------|-----------------------|--------------------------|
| RACS-LOW | 2 665 933 | 2 617 851 | 1 733 301 |
| RACS-MID | 3 107 143 | 3 038 033 | 2 118 761 |
| RACS-HIGH | 3 204 704 | 3 131 871 | 2 455 364 |
| 00-01hour | 2 201 419 | 2 170 113 | 2 169 828 |
| 01-02hour | 119 463 | 117 924 | 117 907 |
| 02-03hour | 1 200 003 | 1 180 784 | 1 180 561 |
| 03-04hour | 478 887 | 467 810 | 467 762 |
| 04-05hour | 137 416 | 134 691 | 134 681 |
| 05-06hour | 573 419 | 563 380 | 563 211 |
| 06-07hour | 1 346 916 | 1 318 819 | 1 318 689 |
| 07-08hour | 190 507 | 187 600 | 187 555 |
| 08-09hour | 734 965 | 725 826 | 725 477 |
| 09-10hour | 229 746 | 225 730 | 225 655 |
| 10-11hour | 2 151 104 | 2 142 785 | 2 141 799 |
| 11-12hour | 91 946 | 88 258 | 88 244 |
| 12-13hour | 105 013 | 103 614 | 103 588 |
| 13-14hour | 38 802 | 38 627 | 38 613 |

bands with centre frequencies of between 700 and 1 700 MHz. We produced combined ASKAP source catalogues from the publicly available SELAVY (Whiting 2012; Whiting & Humphreys 2012) catalogues. Each combined catalogue contained observations with integration times from 0–1 h, 1–2 h, and so on. This is because source density increases with integration time, due to improved sensitivity. As a result, the chance coincidence probability is higher in longer integration observations, and means that a smaller match radius is needed. We removed duplicate sources from each sample by removing sources where the separation was less than the average of the semi-major axis of the two sources. We kept only one instance of each source to prevent multiple crossmatches to a single star, as this would affect our reliability statistics. Table 1 shows the total number of sources in each catalogue.

To reduce contamination from AGN we removed ASKAP sources that were within 2" of a galaxy in the Milliquas (Flesch 2023) and 6dFGSzDR3 (Jones et al. 2005, 2009) catalogues. Milliquas (Million Quasars) is a catalogue of 907 144 quasars and AGN. 6dFGSzDR3 is a catalogue of 125 071 galaxies, including redshifts and velocities for many of them. We also removed resolved ASKAP sources where $S_{\rm int}/S_{\rm peak} > 1.5$, where $S_{\rm int}$ is the integrated flux density and $S_{\rm peak}$ is the peak flux density.

2.2.2 Star catalogue preparation

The four stellar catalogues that we cross-matched the ASKAP source catalogues to are:

 the Fifth Catalogue of Nearby Stars (CNS5; Golovin et al. 2023);

Table 2. Number of sources, N_{star} , in the four star catalogues used for cross-matching.

| Star catalogue | N _{star} | N_{star} (Dec $< +50^{\circ}$) |
|--------------------|-------------------|-----------------------------------|
| CNS5 | 5 908 | 5 193 |
| ROSAT stellar | 27 881 | 23 017 |
| XMM-Newton stellar | 5 042 | 4 400 |
| Wolf-Rayet | 669 | 653 |

- the stellar content of the ROSAT all-sky survey catalogue (Freund et al. 2022, hereafter 'ROSAT stellar');
- the XMM-Newton slew survey (Freund et al. 2018 hereafter 'XMM-Newton stellar');
- the Galactic Wolf-Rayet Catalogue^d (Rosslowe&Crowther 2015).

The number of sources in each is given in Table 2.

The CNS5 is a catalogue of stars within 25 pc of the Sun. It incorporates *Gaia* Early Data Release 3 (EDR3; Gaia Collaboration et al. 2021a; Fabricius et al. 2021) data, Hipparcos data (Perryman et al. 1997) data from ground-based near-infrared surveys. The CNS5 contains 5 931 objects: 5 230 stars (including the Sun) and 701 brown dwarfs. Of the stars, 20 are giant stars, 264 are white dwarfs and 3 760 are M-dwarfs. CNS5 is statistically complete down to 19.7 mag in G-band and 11.8 mag in Wide-field Infrared Survey Explorer (*WISE* Wright et al. 2010) W1-band absolute magnitudes. The white dwarf sample is statistically complete. Golovin et al. (2023) assume that the expected star-to-brown dwarf ratio is ~5, which means that approximately a third of the brown dwarfs within 25 pc of the Sun are yet to be discovered.

The *ROSAT* stellar catalogue is a catalogue of X-ray emitting stars identified by cross-matching between the *ROSAT* All-Sky Survey (RASS; Voges et al. 1999) and the *Gaia* EDR3 catalogue. We use p_{ij} and p_{stellar} , where p_{ij} is the posterior probability that the *j*th counterpart to a *ROSAT* source is the correct identification and p_{stellar} is the probability that the counterpart to the *ROSAT* detection is the correct identification, to include only reliable X-ray identifications. We used only those *ROSAT* stellar sources with $p_{\text{stellar}} > 0.51$ and $p_{ij} > 0.5$ where the completeness and reliability for the cross-matches are over 93%, resulting in a catalogue containing 28 109 sources. We also removed sources flagged as subdwarfs and kept only a single detection for those sources with multiple X-ray detections, resulting in 27 881 sources.

The *XMM-Newton* stellar catalogue contains cross-matches between *XMM-Newton* slew survey sources (Saxton et al. 2008) and stars. It contains 5 920 sources with a completeness of 96.3% and a reliability of 96.7%. We filtered this catalogue by including only one-to-one matches between an *XMM-Newton* source and a star. We excluded those sources that were flagged to have, for example, an accreting object within 30", an AGN within 30", or other issues identified. We did this by excluding sources that had a flag in the Stellar Flag (StFlg) column, as suggested by Saxton et al. (2008). This resulted in a catalogue containing 5 042 stars cross-matched to *XMM-Newton* sources.

The Galactic Wolf-Rayet Catalogue contains 669 Wolf-Rayet stars. We included this catalogue as some Wolf-Rayet stars are

known to emit at radio wavelengths (Dougherty & Williams 2000), such as Apep (Callingham et al. 2019a), WR 48a (Hindson et al. 2012), and HD 93129A (Benaglia et al. 2015)

We prepared each of the star catalogues to make sure they were in a consistent format before cross-matching. For example, some catalogues do not include proper motion information, and others only give a star name, with no further stellar parameters. For each catalogue we used the source names provided by the catalogue to identify the SIMBAD (Wenger et al. 2000a), Gaia DR3 (Gaia Collaboration et al. 2016b, 2023; Babusiaux et al. 2023), DR2 (Gaia Collaboration et al. 2018), and DR1 (Gaia Collaboration et al. 2016a), Tycho (Høg et al. 2000b,a), Hipparcos (Perryman et al. 1997), 2MASS (Skrutskie et al. 2006), GCVS (Samus' et al. 2017), and UCAC4 (Zacharias et al. 2013) names if available. We did this using astroquery SIMBADe to find object IDs based on the object names. We did not attempt position-based identifications as this risks matching to an incorrect source due to proper motion. If we could not find a name-based match, we used the astrometric information from the original catalogue. For example, if we could not find a name for a CNS5 source we used the astrometric information from the CNS5 catalogue itself. For each source we provide the SIMBAD, Gaia DR3 and DR2, Tycho, Hipparcos, 2MASS, GCVS, and UCAC4 names where available. We also provide the astrometric information from one of Gaia DR3, Hipparcos, UCAC4, Gaia DR2, or DR1 for each star. We chose the source of the astrometric information based on which catalogue provided astrometric information. For example, if a source has a Gaia DR3 position and no proper motion, but has a Hipparcos position that does provide proper motion information, we used the Hipparcos information. If the source has a Gaia DR3 position and no proper motion information in any catalogue, then we used the Gaia DR3 position.

2.2.3 Cross-match reliability

We performed Monte Carlo simulations to determine the reliability of the cross-matches and the appropriate cross-match radius to identify radio emission from stars. The cross-match radius is the maximum separation between the centroid of the radio source and the proper motion corrected position of the star.

For the Monte Carlo simulation we used two catalogues, the radio catalogue and the star catalogue. For example, RACS-high as the radio catalogue and the CNS5 as the star catalogue. The simulation was then performed as follows:

- Offset the positions of the stars in a random direction and a random offset magnitude within the range described below.
- 2. Match to the radio catalogue using a cross-match radius of A''
- 3. Count how many cross-matches there are.
- 4. Repeat steps 1 to 3 *M* times for a range of cross-match radii.

For step 1 we offset each star position in the catalogue by taking the square root of a number drawn from a random uniform distribution between c^2 and $(c+r)^2$ where c is the shift and r is the radius. We set c=1' and r=30''. This method means that we are drawing from a random distribution that is uniform over

 $[^]dhttps://pacrowther.staff.shef.ac.uk/WRcat/https://pacrowther.staff.shef.ac.uk/WRcat/.\\$

 $^{^{\}tt e}https://astroquery.readthedocs.io/en/latest/simbad/simbad.html.$

| | CNS5 | | | ROSAT st | | llar | XM | M-Newton : | stellar | | Wolf-Raye | et |
|-----------|--------|--------|---------|----------------------|--------|---------|--------|------------|---------|--------|-----------|--------|
| ASKAP | 98% | Match | Num. of | 98% | Match | Num. of | 98% | Match | Num. of | 98% | Match | Num. |
| Catalogue | radius | radius | matches | radius | radius | matches | radius | radius | matches | radius | radius | matche |
| RACS-high | 3.4" | 3.4" | 50 | 3.5" | 3.5" | 263 | 5.2" | 4.0" | 115 | 6.2" | 4.0" | 13 |
| RACS-low | 2.3" | 2.3" | 16 | 0.8" | - | - | 2.7" | 2.7" | 24 | - | - | - |
| RACS-mid | 3.1" | 3.1" | 37 | 3.2" | 3.2" | 181 | 4.4" | 4.0" | 74 | 5.8" | 4.0" | 9 |
| 00-01hour | 3.3" | 3.3" | 44 | 2.7" | 2.7" | 125 | 3.6" | 3.6" | 54 | 2.0" | 2.0" | 6 |
| 01-02hour | 5.7" | 4.0" | 4 | 3.8" | 3.8" | 8 | 6.7" | 4.0" | 4 | 3.5" | 3.5" | 1 |
| 02-03hour | 3.0" | 3.0" | 18 | 2.4" | 2.4" | 36 | 3.6" | 3.6" | 19 | - | - | - |
| 03-04hour | 1.1" | - | - | $0.9^{\prime\prime}$ | - | - | 2.6" | 2.6" | 4 | 8.7" | 4.0" | 1 |
| 04-05hour | 2.0" | 2.0" | 1 | 1.9" | - | - | 2.3" | 2.3" | 1 | - | - | - |
| 05-06hour | 2.2" | 2.2" | 5 | 2.7" | 2.7" | 23 | 4.2" | 4.0" | 11 | 3.3" | 3.3" | 3 |
| 06-07hour | 2.7" | 2.7" | 17 | 1.9" | - | - | 3.3" | 3.3" | 26 | 5.7" | 4.0" | 4 |
| 07-08hour | 3.7" | 3.7" | 4 | 3.7" | 3.7" | 11 | 4.5" | 4.0" | 5 | - | - | - |
| 08-09hour | 2.3" | 2.3" | 7 | 3.9" | 3.9" | 61 | 5.1" | 4.0" | 23 | 24.9" | 4.0" | 0 |
| 09-10hour | 3.0" | 3.0" | 4 | 2.4" | 2.4" | 7 | 3.9" | 3.9" | 4 | - | - | - |
| 10-11hour | 2.1" | 2.1" | 16 | 2.8" | 2.8" | 150 | 3.8" | 3.8" | 83 | 4.3" | 4.0" | 6 |
| 11-12hour | 17.0" | 4.0" | 0 | 2.1" | 2.1" | 2 | 3.7" | 3.7" | 1 | - | - | - |
| 12-13hour | 3.3" | 3.3" | 2 | 0.8" | _ | _ | 2.5" | 2.5" | 3 | _ | _ | _ |

4 5

4 0

Table 3. Results of the Monte Carlo analysis and ASKAP-star catalogue cross-matches. For each ASKAP-star catalogue cross-match we show the 98% radius, the cross-match radius used, and the number of matches found.

the area of an annulus around each star. We chose this minimum shift value such that we reduced the number of real matches contaminating our random cross-matches. For step 2 we used the cumulative number of matches. For example, we counted how many matches there were within 1", then 2" and so on. In step 3 we used a one-to-one matching, so each radio source and each star was only counted once. We matched in radius bins up to 30" with 0'.1 bins. In step 4 we repeated this process for each radio catalogue cross-matched to each star catalogue (shown in Table 3). We repeated it 100 000 times each. We did not take proper motion into account for the Monte Carlo simulations as the density of sources on the sky is more important than the true positions.

13-14hour

We calculated the mean value, λ , in each radius bin. This gives us the expected number of random matches per radius bin for the cross-match between both complete catalogues. This method assumes that none of the matches between the radio catalogue and randomised star catalogue are true matches. An example of the cumulative number of matches per bin for a cross-match between RACS-high and CNS5 is shown in Fig. 1.

We also performed the binned cross-match between the radio catalogues and the true, proper motion corrected positions of the objects from the star catalogues. We could then calculate the reliability of the cross-matches at different radii up to 30". The results of this cross-match between RACS-high and CNS5 are also shown in Fig. 1.

The reliability at a given cross-match radius is given by $R = 1 - N_{\rm random}/N_{\rm true}$, where R is the reliability, $N_{\rm true}$ is the number of matches at a given radius using the true coordinates for both catalogues and $N_{\rm random}$ is the number of matches at a given radius as a result of the 100 000 iteration Monte Carlo simulation.

We selected the match radius for each radio-star catalogue cross-match, such that the resultant reliability was 98%. The radius

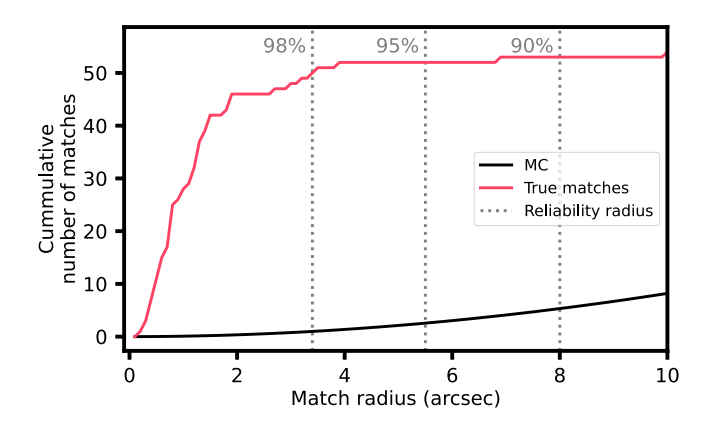


Figure 1. Example cumulative cross-match plot for the cross-match between the CNS5 catalogue and RACS-high. We show the results of the 100 000 iteration Monte Carlo simulation and the true, proper motion corrected cross-match. The match radii for 90, 95, and 98% reliability is also shown here.

that this corresponds to for each pair of catalogues is shown in Table 3. The typical uncertainty on ASKAP source positions is 2". In some cases the 98% reliable match radius is larger than 2" due to the low density of sources in one or both of the catalogues. In these cases we used up to twice the typical ASKAP position uncertainty as the cross-match radius: 4". For cases where the cross-match radius required for 98% reliability was less than the ASKAP position uncertainty of 2" we did not perform a cross-match. In some cases there are no matches within 30" of any of the source positions. Those cases have been left blank. The Wolf-Rayet catalogue includes the fewest sources so there are many cases where there are no cross-matches between the Wolf-Rayet source catalogue and

the ASKAP source catalogue. This means that the smallest crossmatch radius we used was 2" and the largest cross-match radius we used was 4".

2.2.4 Results

We used the cross-match radii shown in Table 3 to cross-match between each radio catalogue and each star catalogue. The results of the cross-matches are shown in the third sub-columns in Table 3. Note that there is some overlap between the results of the cross-matches. For example, a star might be found in the cross-match between RACS-high and CNS5 and that same star might have been found in the cross-match between RACS-low and the *ROSAT* star catalogue.

We performed final checks by checking the SIMBAD object type of each source. HD 8357 (also known as AR Psc) and TWA 22 were both identified by Simbad as X-ray binaries. However, AR Psc is an RS CVn binary consisting of a K1 subgiant and a G7V dwarf (Fekel 1996; Kawai et al. 2022) and TWA 22 is an M dwarf binary where both component are \sim M5 stars (Rodet et al. 2018). We have therefore kept both of these objects in the SRSC.

We removed Gaia DR3 247993683714250368 as it had an uncharacteristically high radio luminosity for a radio star: it is on the main sequence and is not a Wolf-Rayet star; however, its radio luminosity was calculated to be $\sim 10^{19} \, \mathrm{erg \, s^{-1} \, Hz^{-1}}$. This is approximately two orders of magnitude higher than expected for this star, which we noticed as a clear outlier in luminosity in the CMD. Only some of the Wolf-Rayet stars in the sample have similar luminosities. The radio spectrum from Stein et al. (2021) shows a power law spectrum with a spectral index of ~ -0.7 . In this case, there is an optical star in front of a radio- and X-ray loud AGN.

We removed the Wolf-Rayet star CXOGC J174528.6—285605 after visually inspecting the ASKAP images, as the radio detection of this source appears to be slightly resolved. We also removed WR 76-6, WR 76-7, and WR 76-8 because these Wolf-Rayet systems were all matched to the same radio source as they are closely colocated on the sky and we could not distinguish which system was responsible for the radio emission.

There are two pairs of *Gaia* sources:

• Gaia DR3 4105057482987021184 and

Gaia DR3 4105057482994688384;

• Gaia DR3 6130530322820978304 and

Gaia DR3 6130530322823774720

where both sources in the pair were identified as the same radio source due to the small separation between the Gaia sources. Both pairs were identified as radio stars using the Stokes V search method. After examining the Gaia parameters for the pairs, both objects in each pair have near-identical proper motion and parallax values. This means that they are likely binary systems. As such we have kept these pairs of sources in the SRSC.

Performing these checks and removing the sources described above resulted in 727 unique stars.

2.3 Other data and samples

We have included in the SRSC the 37 radio stars in V-LoTSS found via circular polarisation searches of LoTSS data (Callingham et al. 2023) and the 22 stars found by cross-matching V-LoTSS and the

GCNS from Yiu et al. (2024). We also included the 25 and 65 stars found by cross-matching LoTSS and VLASS, respectively, to the GCNS (Yiu et al. 2024).

We have included stars found in searches for variable radio sources using ASKAP and MeerKAT. The ASKAP stars presented here were found byWang et al. (2023) using the VAST short time scale imaging pipeline. They found eight stars with radio variability on minute timescales. Three MeerKAT-detected stars have been included in the catalogue:

- MKT J170456.2-482100 (Driessen et al. 2020),
- EXO 040830-7134.7 (Driessen et al. 2022), and
- SCR 1746-3214 (Andersson et al. 2022).

All of these stars were found in untargeted searches for radio variability as part of the ThunderKAT project (Fender et al. 2016). We have included the eight stars found in proper motion searches by Driessen et al. (2023); two of the eight sources had not previously been identified as radio stars.

2.4 Samples that are not included

In this version of the SRSC we have included reliable identifications of radio stars from wide-field searches for radio stars using SKA precursors and pathfinders. We have not included candidate radio stars, such as the two tentative detections made by Lenc et al. (2018) using the Murchison Wide Field Array (MWA; Tingay et al. 2012).

We plan to perform a detailed literature search in the near future for detections from other searches and studies of radio stars, such as Suresh et al. (2020), Villadsen & Hallinan (2019) and more. We plan to include these stars in a future version of the SRSC. Part of this literature search will include confirming the reliability of past detections, as some stars in e.g. the CRS were considered candidate detections but were still included as radio stars. We encourage submissions to the SRSC via email to the corresponding author.

We do not plan to include identification of stars in the mmband, such as the detections using the South Pole Telescope (SPT; Guns et al. 2021; Whitehorn et al. 2016) by Tandoi et al. (2024). This is because detections at these higher frequencies probe different physics to MHz/GHz radio detections.

3. Catalogue format

The SRSC consists of two tables, the stars table and the radio table. The stars table contains the identification information and basic properties of each unique star in the catalogue: there is one row per star. The radio table contains data for each radio measurement of each star in the catalogue: there may be more than one row per star. Both tables contain a unique identifier for each star of the format SRSC XXXXXX to link the information in the tables together. The columns in the star table are described in Table 4 and the columns in the radio table are described in Table 5.

The astrometric information for the stars in the stars table is provided by the survey in the survey column. As described in Section 2.2.2, the preferred survey for this information is *Gaia* DR3; however, preference is given to the survey which includes proper motion information. We did not attempt to cross-identify sources between surveys based on source position because this is prone to misidentification. The different names for the stars are

Table 4. Description and units of the columns in the star table.

| Column name | Units | Description |
|-----------------------|--------|---|
| Identifier | | A unique identifier for each star in the SRSC. |
| SIMBAD | | The main identifier from the CDS SIMBAD database (Wenger et al., 2000a). |
| Gaia | | <i>Gaia</i> unique source identifier (unique within a particular Data Release, Gaia Collaboration et al., 2016b, 2023; Babusiaux et al., 2023). For this release of the SRSC the <i>Gaia</i> identifier is from DR3 |
| Tycho | | TYC1-3 (TYC number) Tycho identifier (Høg et al., 2000b,a). |
| MASS | | 2MASS designation from the Two Micron All Sky Survey at IPAC (Skrutskie et al., 2006). |
| GCVS | | Designation from the General Catalogue of Variable Stars (GCVS) (Samus' et al., 2017). |
| HIP | | Hipparcos input catalogue running number (Perryman et al., 1997). |
| UCAC4 | | Recommended identifier from the Fourth U.S. Naval Observatory CCD Astrograph Catalog (Zacharias et al., 2013). |
| Survey | | The survey used to provide the astrometric information shown here (i.e. the position, proper-motion and parallax information) |
| Survey_id | | Designation of the source in the survey used to provide the astrometric information for the source |
| Epoch | jyear | The observation epoch of the source in the survey. The RA and Dec provided here is proper-motion correct/observed, all RA and Dec are in the J2000 reference frame |
| RAdeg | degree | The J2000 RA in degrees proper-motion corrected to the date in the 'Epoch' column |
| e_RAdeg | mas | The uncertainty on the Right Ascension |
| DEdeg | degree | The J2000 Declination in degrees proper-motion corrected to the date in the 'Epoch' column |
| e_DEdeg | mas | The uncertainty on the Declination |
| plx | mas | The parallax provided by the survey |
| e_plx | mas | The uncertainty on the parallax |
| pmRA | mas/yr | The proper-motion in Right Ascension (\times cos (Dec)). |
| e_pmRA | mas/yr | The uncertainty on the proper-motion in Right Ascension (\times cos (Dec)) |
| pmDE | mas/yr | The proper-motion in Declination |
| e_pmDE | mas/yr | The uncertainty on the proper-motion in Declination |
| Identification_method | | Indicates the search methods used to identify the radio emission as stellar emission from this star. The possible values are the sum of cross-match $= 2$, variability $= 4$, proper-motion $= 8$, and Stokes $V = 16$. For example, a source found in both a cross-match and Stokes $V = 16$ search would have a value of $2 + 16 = 18$ |
| Radio_multiple | | Flag indicating multiple optical matches to one radio source. 0 indicates that there is only one optical match to the radio component. Values of 1 and 2 indicate that there are multiple matches, where 1 is the 'preferred' source and 2 is a 'duplicate'. This is for ease of use, such that selecting rows where this flag = 0 or 1 results in a set of one-to-one radio to optical matches. If one radio component has multiple optical matches this indicates that the optical matches are multiple components of the same stellar system |

from SIMBAD, or were included if there was a cross-identification in the original survey information. For example, *Gaia* source information does sometimes include the Tycho or 2MASS identification of a star.

The identification_method column in the stars table provides a binary flag to indicate which search methods were used to identify the star as a radio star. This means that the user can filter the catalogue based on search method. The radio_multiple flag in the stars table indicates whether the radio-star crossmatch has a one-to-one match or a one-to-many match. This is because the typical uncertainty on radio positions is larger than the separation between the components of some binary systems. ASKAP has typical astrometric accuracy of 1" - 2", LoTSS 0'.2, VLASS 0'.5, and MeerKAT 1". This means that there may be one radio detection that is matched to both components of a binary system. Where there is a one-to-many match between one radio source and more than one star, we have set the radio_multiple flag for the 'preferred' star to 1 and we have set the flag for the 'duplicate' star to 2. The 'preferred' star is either the system identification, e.g. AT Mic instead of AT Mic A and AT Mic B, or

the 'A' component of the system. One-to-one matches have a $radio_multiple$ flag of 0.

In the search described in Section 2.2 we removed possible repeat detections to correctly calculate the cross-match reliability. However, since there are repeat ASKAP observations of many areas of sky, many of the stars are likely to have repeat detections. Using the list of unique stars in the stars table, we searched all public ASKAP data up to 2024 March 26 to find repeat detections of these stars, using a match radius of 4". We have only included detections in the catalogue, not upper limits. All detections of stars table sources are in the radio table. We show excerpts of the stars table (Table A1) and radio table (Table A2) in Appendix 1.

The catalogue presented here is the first version of the SRSC. A static version of the catalogue is available in Vizier. It contains the stars presented in this paper. We will

^fAvailable at CDS via anonymous ftp to cdsarc.u-strasbg.fr (130.79.128.5) or via https://url.au.m.mimecastprotect.com/s/PjB4CzvkyVC8LWjqxI4iLF_?domain=cdsarc.cds.unistra.fr.

Table 5. Description and units of the columns in the radio table.

| Column name | Units | Description |
|------------------|----------|--|
| Identifier | | A unique identifier for each star in the SRSC |
| Telescope | | The radio telescope used for the observation |
| Survey | | Name of the radio survey in which the star was identified |
| Match_separation | arcec | The separation between the radio and optical position, where the optical position has been proper motion corrected to the epoch of the radio observation |
| Radio_id | | The identifier/name of the radio source in the radio survey |
| Field | | The designation/identifier of the radio field or observation in the radio survey |
| Obs_date | ISOT | ISOT start time of the radio observation |
| Exposure | S | Integration time of the radio observation |
| RAdeg | degree | The Right Ascension in degrees of the source in the radio observation |
| DEdeg | degree | The Declination in degrees of the source in the radio observation. |
| e_RAdeg | arcsec | The uncertainty on the Right Ascension |
| e_DEdeg | arcsec | The uncertainty on the Declination |
| Freq | MHz | The central frequency of the radio observation |
| Speakl | mJy/beam | The peak flux density of the Stokes I detection of the source |
| e_SpeakI | mJy/beam | The uncertainty on the peak flux density of the Stokes I detection of the source |
| Stotl | mJy | The integrated flux density of the Stokes I detection of the source |
| e_Stotl | mJy | The uncertainty on the integrated flux density of the Stokes I detection of the source |
| bmax | arcsec | The major axis of the synthesised beam |
| bmin | arcsec | The minor axis of the synthesised beam |
| PA | degree | The position angle of the synthesised beam |
| e_bmax | arcsec | Uncertainty on the major axis of the synthesised beam |
| e_bmin | arcsec | Uncertainty on the major axis of the synthesised beam |
| SpeakV | mJy/beam | The peak flux density of the Stokes V detection of the source |
| e_SpeakV | mJy/beam | The uncertainty on the peak flux density of the Stokes V detection of the source |
| StotV | mJy | The integrated flux density of the Stokes V detection of the source |
| e_StotV | mJy | The uncertainty on the integrated flux density of the Stokes V detection of the source. |
| localrmsV | mJy/beam | The local Stokes I rms |
| localrmsI | mJy/beam | The local Stokes V rms |
| Ref | | The reference (bibcode) for the radio star identification |

maintain and update a version of the catalogue on the website https://radiostars.org/.

4. Properties of radio stars in the SRSC

The current version of the SRSC comprises 839 unique stars with 3 405 total radio detections (398 stars have a single radio detection while 441 have more than one) at frequencies from 144 MHz to 3 GHz. The sky distribution of the stars is shown in Fig. 2. The stars are distributed across the whole sky; with $\sim\!74\%$ at Dec< 0°. This is because nearly 75% of ASKAP observations are of this region and $\sim\!95\%$ of the stars in the SRSC have been detected at least once using ASKAP. The integrated flux densities over all radio detections range from 0.02 mJy (EXO 040830–7134.7) to 199.4 mJy (Apep).

A distance measurement is needed to calculate the luminosities of the stars in the SRSC. We used the rgeo distance measurements from Bailer-Jones et al. (2021) to calculate the luminosities for the SRSC stars. 800 of the 839 stars have an rgeo distance measurement. The nearest star is Proxima Centauri (at 1.3 pc) and the most

distant star is WRAY 15-682 (also known as TYC 8958-1166-1, at 7 315 pc), both of which have been detected in the radio before (Haisch et al. 1978; Duncan & White 2002).

The number of stars detected using the different methods is shown in Fig. 3, with the proper motion detected (8 total) and variability detected (9 total) stars combined into one set due to their comparatively low numbers. The different numbers of stars found using the different search methods is caused by a combination of factors. Radio stars can emit radio flares, persistent quiescent emission, or both. The circular polarisation search method presented here was applied to a limited set of 12-15 min ASKAP observations, and circularly polsarised emission is typically from stellar flares. Similarly, the ASKAP variability search was applied to a limited set of observations and was sensitive to flares. The proper motion search method was applied to sources covered by both FIRST and RACS and depends on each star being detected at least twice. This means that this method was limited to stars that are persistent radio emitters or flare more often. All three of these methods used short integration time radio images, limiting their sensitivity to faint radio emission. Conversely, the cross-match

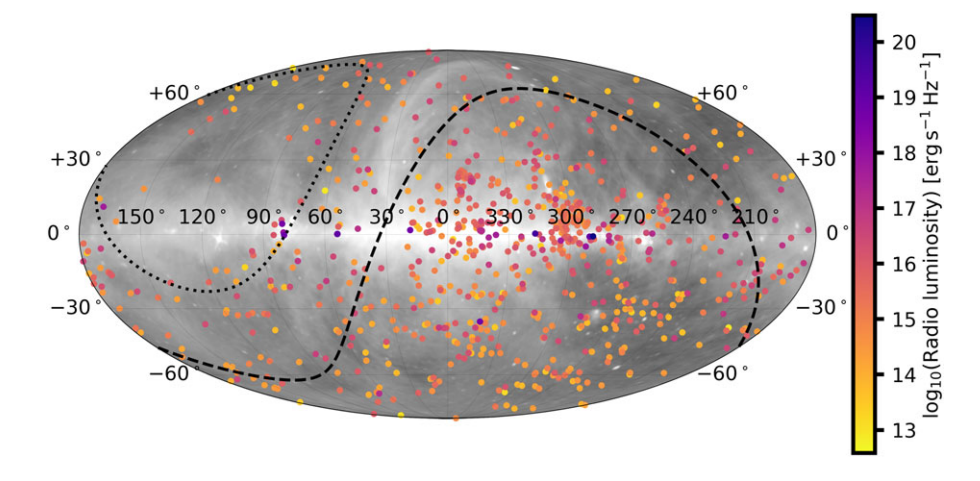


Figure 2. Sky map showing the positions of the SRSC stars in Galactic coordinates. The stars are coloured by their maximum radio luminosity. The black dashed line indicates $Declination = 0^{\circ}$ and the black dotted line indicates $Declination = +40^{\circ}$.

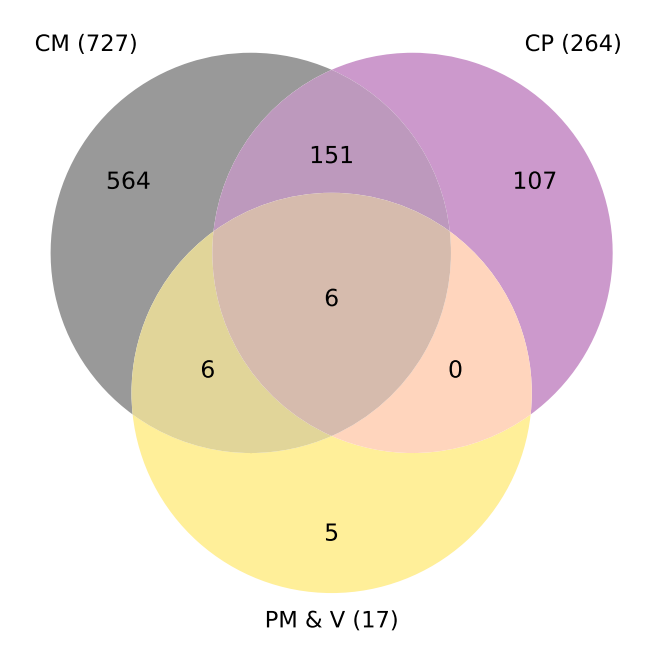


Figure 3. Number of sources detected using the cross-match (CM), circular polarisation (CP) and proper motion and variability (PM & V) methods.

search method was applied to all Stokes I ASKAP observations with integration times from minutes to hours. This method was therefore sensitive to both flaring and persistent emission. As well as these search method and observational biases, the SRSC only includes detections below 3 GHz where non-thermal emission dominates.

The variety of methods used to compile the SRSC make determining the completeness of the sample challenging. However, Pritchard et al. (2024) showed that late-type dwarfs have a high-degree of variability. This means that the future, repeat ASKAP observations as part of RACS, VAST and general observing will improve the completeness of the catalogue. We only included sources with reliability >98% when cross-matching (see Section 2.2.3) and the reliability of the circular polarisation, variability and proper motion searches is expected to be higher. However, the cross-match reliability is also determined by the reliability of the underlying star catalogue used. The reliability of

the *ROSAT* stellar catalogue is 93% (Freund et al. 2022) and the reliability of the *XMM-Newton* stellar catalogue is 96.7% (Freund et al. 2018). These reliabilities should be taken into account when using the SRSC. The Identification_method column, which indicates the search method/s used to identify each object in the SRSC, will assist users in assessing the reliability of each object identification.

4.1 Colour-magnitude diagram

Colour-magnitude diagrams are a useful tool for giving an overview of the types of stars in a sample. This has previously been demonstrated for radio stars using the CRS by Güdel (2002, using 440 radio stars detected a \leq 10 GHz) and more recent work by Pritchard et al. (2021, using 231 radio stars detected at \leq 10 Hz). These works showed that stars across the Hertzsprung-Russell (HR) diagram are radio stars; however, the CRS contained radio detections of stars from 1–10 GHz. This means that these HR diagrams show a mix of thermal and non-thermal stellar radio emission. Figure 2 in Pritchard et al. (2021) demonstrated that cool stars were detected at lower frequencies while hotter stars and subgiant and giant stars were detected at higher frequencies.

We used the set of stars that have Gaia DR3 magnitudes and rgeo distances to create a CMD of the stars in the SRSC, shown in Fig. 4. M_G is the absolute G-band (\sim 330–1 050 nm) magnitude and G_{RP} and G_{RP} are the Gaia blue (330–680 nm) and red (640–1 050 nm) apparent magnitudes. Fig. 4 shows that there are radio detected stars across the CMD. Compared to the previous studies using the CRS, the stars in the SRSC are all detected below 3 GHz, with the majority detected below 2 GHz using ASKAP, where nonthermal radio emission dominates. We can see that stars that have a brighter M_G are also more radio luminous. There is a large cluster of stars on the sub-giant part of the red giant branch and some stars are in the red clump. These sub-giant stars are more radio luminous than the main sequence stars. We can also see that many of the stars are above the lower main sequence. Many of these are known to be pre-main-sequence stars, such as T Tauri stars and Orion variables. These stars tend to be more radio luminous than the stars on the main sequence at a similar M_G . The cool dwarfs, the stars on the main sequence with the faintest M_G , have the lowest radio luminosities. This means that we are detecting a

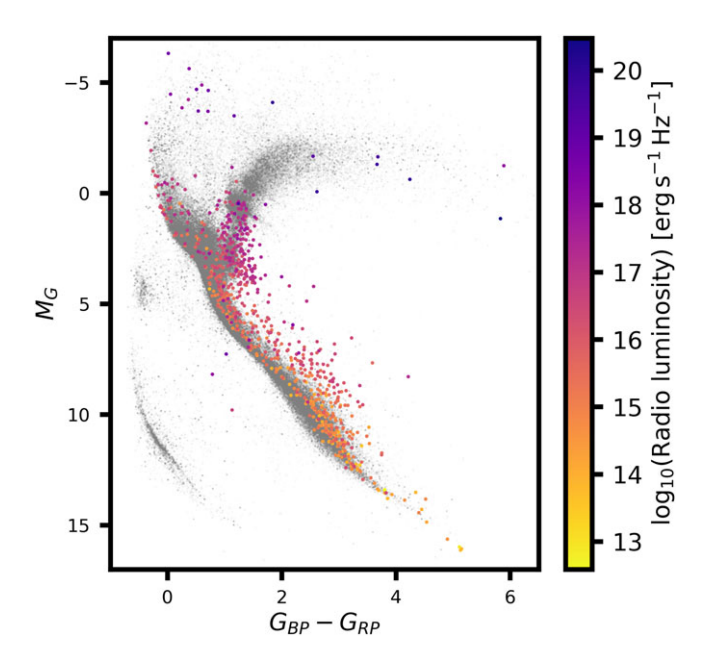


Figure 4. *Gaia* DR3 CMD showing the radio stars in the SRSC in colour. The colour scale shows the radio luminosity based on the maximum flux density of each star in the SRSC and the *Gaia* \mathbf{x} geo distance. The grey background points show the *Gaia* DR2 CMD for reference (Pedersen et al. 2019).

closer-by sample than the sample of sub-giant and giant stars that are brighter in the radio.

There are ten objects in the SRSC that do not have a *Gaia* identifier from any data release. Sources are not in *Gaia* when they are either too faint (e.g. ultracool dwarfs), too bright, or in a crowded region. Three of the ten objects without *Gaia* identifiers are ultracool dwarfs: 2MASS J09481615+5114518, 2MASS J10534129+5253040 and [VCS2020] BDR J1750+3809. The other seven objects include the bright star (magnitude \sim 1.5) Castor AB and the Wolf-Rayet stars Regor, [KSF2015] 1256–1483A, and Apep that are too bright to be in *Gaia*. The remaining objects are UPM J1709–5957, 1RXS J200031.8+592127, and V503 Hya. It may be that they are binary systems so the individual stars have *Gaia* identifiers but not the system. Or there may be two *Gaia* sources close to the star and so they have not been linked to either of them in SIMBAD or other catalogues.

4.1.1 M dwarfs

M dwarfs are one of the most common types of detectable radio star. There are 208 stars in the SRSC that are classified in SIMBAD as either a single star of 'M' spectral type, or a binary with at least one 'M' spectral type component. Just over half of these stars, 106, are detected in the radio more than once. Since there are many M dwarfs with multiple detections we are unable to show all the light curves here. We show the light curves of the fourteen M dwarfs with ten or more radio detections in Fig. 5. We can see that these stars are highly variable in the radio, with some higher flux density detections that may indicate bursts or flares.

4.1.2 Stars below the main sequence

There are three stars in the SRSC that fall below the main-sequence in the CMD in Fig. 4: the cataclysmic binary 2MASS J19551247+0045365 (also known as J19552+0044; Masetti et al. 2010; Bernardini et al. 2013), and *Gaia* sources Gaia DR3 1846427022035230592 and 961025698716736768. Stars in this

area of the CMD are often binary systems with a white dwarf component or B-type subdwarfs.

2MASS J19551247+0045365 is an asynchronous short-period polar type CV (Tovmassian et al. 2017). The white dwarf component has a magnetic field below 20 MG and a spin period of 81.29 ± 0.01 m, while the binary system has an orbital period of 83.599 ± 0.002 m. 2MASS J19551247+0045365 is a known radio source (Barrett et al. 2020). Barrett et al. (2020) observed it using the VLA X-band (8–12 GHz) and detected a flux density of 0.073 ± 0.007 mJy. We detect the source twice with flux densities of 2.2 ± 0.03 ($|S_V|/S_I = 68\%$) and 1.6 ± 0.2 mJy (no Stokes V measurement taken) at 887.5 and 943.5 MHz, respectively.

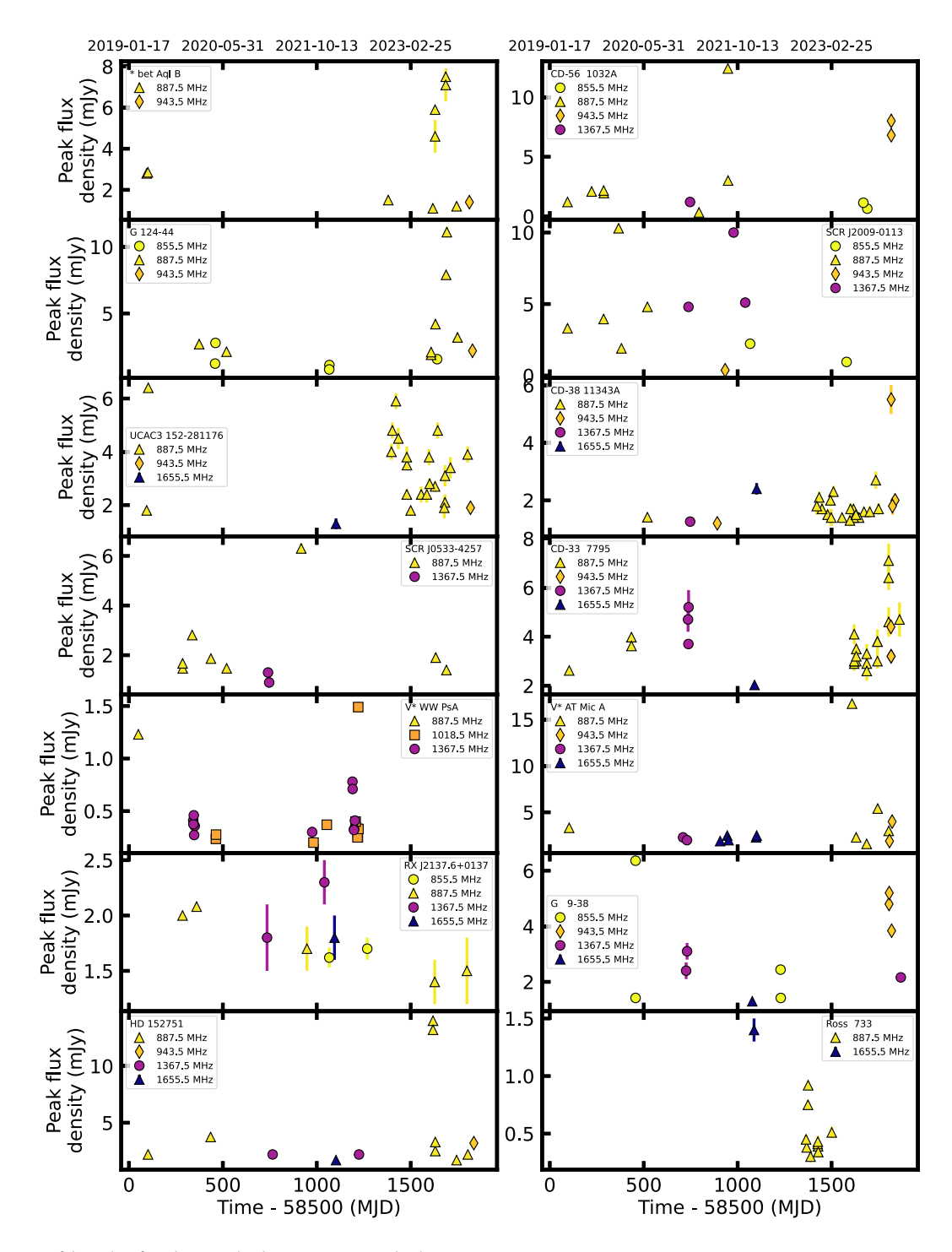
The other two sources are not well studied and have not previously been identified as radio stars. Further investigation is required to identify their stellar type and determine if they are white dwarf binary systems. All three of these sources were found in the circular polarisation search described in Section 2.1. Gaia DR3 1846427022035230592 and Gaia DR3 961025698716736768 have each only been detected once in the radio, in RACS-high, with flux densities 1.7 ± 0.2 mJy ($|S_V|/S_I = 67\%$) and 1.1 ± 0.2 mJy ($|S_V|/S_I = 72\%$), respectively.

4.1.3 Luminous radio stars and Wolf-Rayet systems

The most radio luminous stars are in the top left of the CMD (brighter M_G) as well as on the giant branch. These stars include Wolf-Rayet stars, symbiotic binaries, and blue supergiants. We selected these stars by choosing stars where the SIMBAD main classification is 'WolfRayet*', or where $G_{BP} - G_{RP} > 2.5$ and M_G < 2, or where M_G > 2. There are a total of 24 stars that meet one or more of these criteria and fourteen of those stars have been detected three times or more in the radio. The light curves of the fourteen luminous radio stars that have been detected three or more times are shown in Fig. 6. We can see that these stars are highly variable. HD 167971 (also known as MY Ser) has a particularly interesting light curve. MY Ser is a hierarchical triple system at a distance of 1.8 kpc. It consists of a 3.3 day binary (O7.5III+9.5III) with a third component (O8I) in a 21.4 yr orbit. It is a well-known non-thermal radio source. It has been observed to have long-term radio variability on time scales of years (e.g. Blomme et al. 2007). We can see in its light curve that the flux density of MY Ser has been steadily declining over approximately a year. The ten stars that are detected only once or twice are λ Lep, θ Mus, HD 148937, HD 86161, HD 96548, Schulte 9, HD 152408, IPHAS J193038.84+183909.8, HD 156385 and HD 152270.

4.2 Güdel-Benz relation

The Güdel–Benz relation is the correlation between the radio (5–9 GHz) and X-ray (soft, \sim 0.1–2.4 keV) luminosity of coronally active stars (Güdel & Benz 1993). Past investigations of this relation at a range of frequencies have typically demonstrated it using a few tens of stars (e.g. Callingham et al. 2021; Vedantham et al. 2022; Yiu et al. 2024). The original relation was given by $L_X/L_R \approx 10^{15.5}$ where L_R and L_X are the quiescent radio specific and X-ray luminosities, respectively (Güdel & Benz 1993). A more recent version is now commonly used, where $\log_{10} [L_R] = 1.36 \left(\log_{10} [L_X] - 18.96\right)$ (Williams, Cook, & Berger 2014). The Güdel–Benz relation implies that the mechanism that accelerates non-thermal electrons and the mechanism that heats the corona are the same.



 $\textbf{Figure 5.} \ Light curves of the \ M \ dwarfs in the \ SRSC \ that \ have ten \ or \ more \ radio \ detections. \ MJD \ 58500 \ is \ 2019 \ January \ 17.$

The Güdel-Benz relation has been demonstrated to apply to incoherent, gyrosynchtrotron emission from RS CVns, single active cool dwarfs, BY Draconis binaries, and solar flares. At lower frequencies than 5 GHz, it has been demonstrated that the Güdel-Benz relation no longer applies for some stars (Callingham et al. 2021) because the radio emission arises from coherent mechanisms, as coherent radio emission is more luminous and does not contribute to heating the corona. However, some coherently-emitting radio stars do still follow the relation closely (Vedantham et al. 2022).

The SRSC more than doubles the known number of radio stars, making it an excellent sample to further investigate the Güdel-Benz relation. To this end, it is important to complement the SRSC with a sensitive large scale X-ray survey. Such a survey is now provided with the eROSITA (extended ROentgen Survey with an Imaging Telescope Array, Predehl et al. 2021), the soft X-ray instrument onboard the SRG spacecraft.

eROSITA (Predehl et al. 2021) performed a deep all-sky survey in the 0.2–10.0 keV energy range. The eROSITA all-sky survey (eRASS) data is accumulated in successive all-sky surveys with a

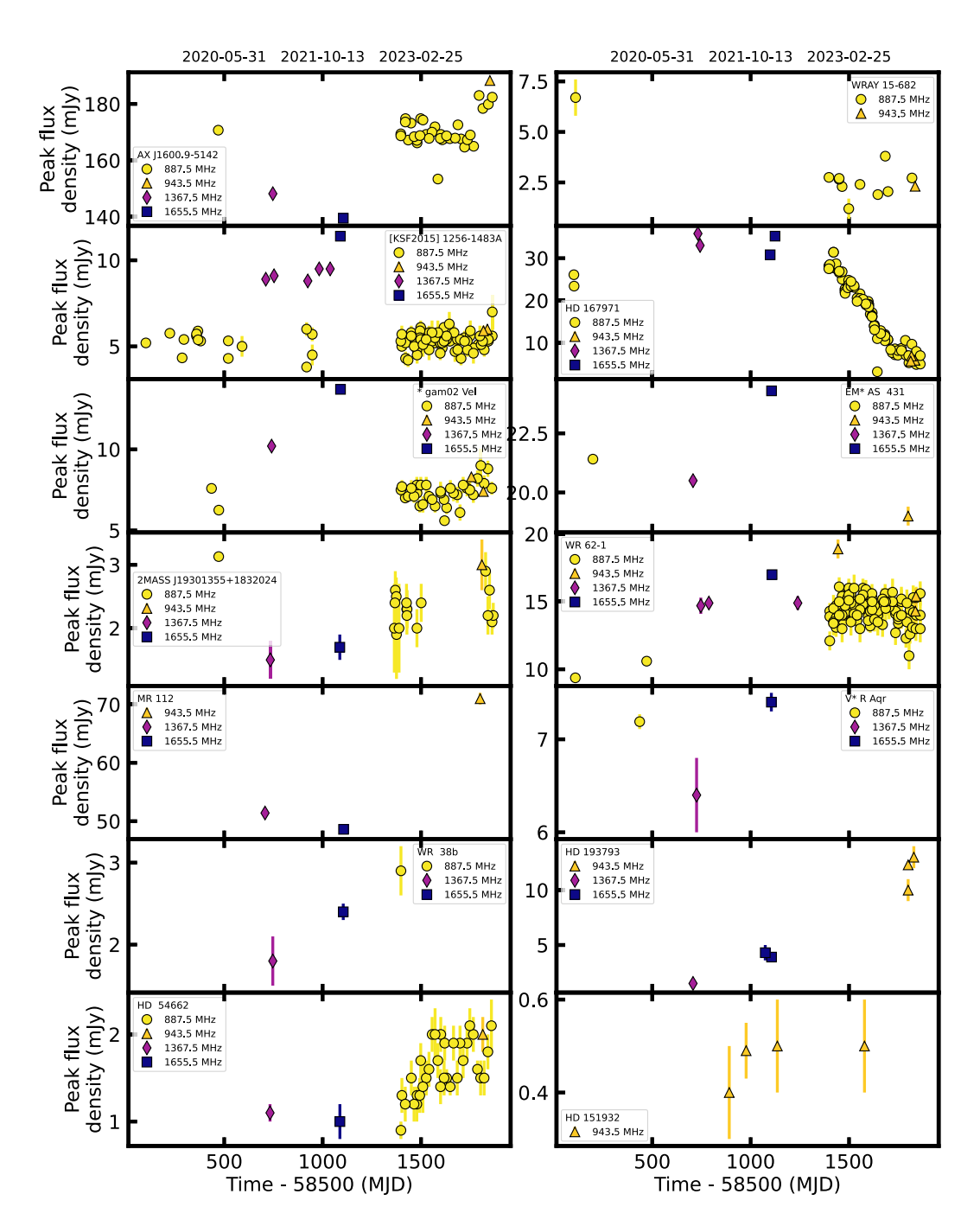


Figure 6. Radio light curves of the luminous radio stars and Wolf-Rayet stars in the SRSC that have been detected three or more times. MJD 58500 is 2019 January 17.

duration of about 0.5 yr each. The DR1 data release of the eRASS1, that contains the first half-year of data from the western Galactic hemisphere and a description of the survey, instrument performance as well as data products and source catalogues are presented in Merloni et al. (2024). For our analysis we use the X-ray catalogue from the more sensitive, accumulated data from the first four all-sky surveys (eRASS:4, 2 yr data, version c020/221031, currently available to the eROSITA_DE consortium) and performed a positional cross-match with the SRSC sample, using a matching radius of 10". The matching radius was adapted to the average positional uncertainty of eROSITA, while likewise keeping the number of false positives at an acceptable level, in this case below 1%.

Note that this eRASS catalogue covers only half of the sky, roughly $l \ge 180$ deg. The adopted X-ray fluxes are survey averages and refer to the standard eROSITA energy band of 0.2–2.3 keV.

We show the SRSC radio luminosities and eROSITA X-ray luminosities for the SRSC stars in the top panel of Fig. 7. The western Galactic hemisphere is largely in the southern sky, the same area that is well covered by ASKAP. There are 800 stars in the SRSC with *Gaia* rgeo distance measurements, and 530 of those have eROSITA X-ray detections. We show the *ROSAT* X-ray luminosities for the SRSC stars in the bottom panel of Fig. 7. The *ROSAT* luminosities are from the *ROSAT* stellar catalogue used for cross-matching in Section 2.2. 616 of the stars with a *Gaia*

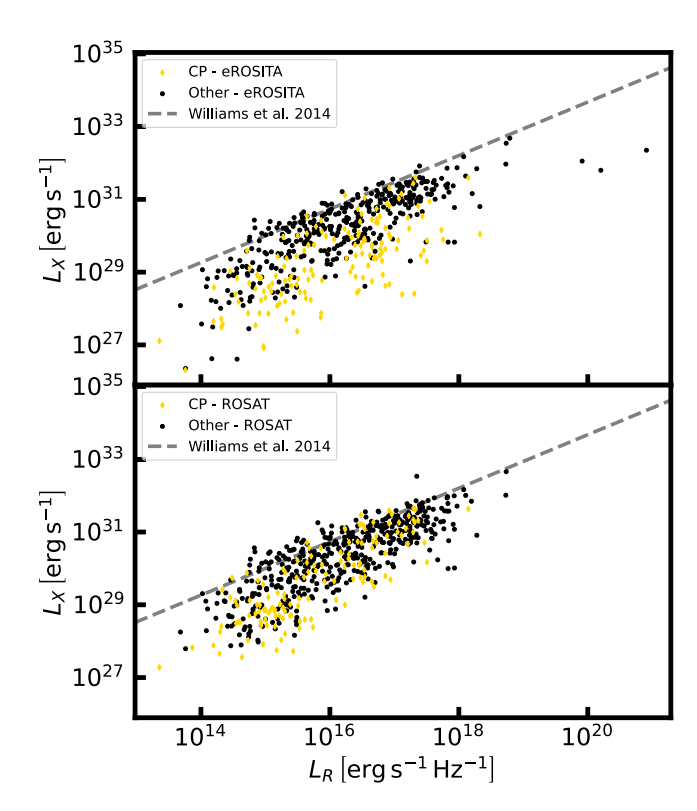


Figure 7. Güdel–Benz plot showing the radio stars in the SRSC. The X-ray luminosity in the top panel is from eROSITA and the X-ray luminosity in the bottom panel is from *ROSAT*. We show the stars that were found using the circular polarisation method (CP), and the stars that were found using other methods (other). Each star is only present once in each panel. The grey-dashed line shows the Güdel–Benz relation from Williams et al. (2014).

rgeo distance measurement have a *ROSAT* X-ray detection, 429 of those *ROSAT* detections are within the region of sky covered by eROSITA. This means that eROSITA has detected 101 more stars than ROSAT (a ~120% increase) in the same sky area as ROSAT. 260 of the stars with a *Gaia* rgeo distance measurement have an *XMM-Newton* detection in the *XMM-Newton* Stellar catalogue used for cross-matching in Section 2.2.

We can see in both panels of Fig. 7 that most stars in the SRSC are over-luminous in the radio (or under-luminous in the X-ray) compared to the expected correlation. This has been noted before using both LOFAR (~200 MHz) and VLASS (3 GHz). Yiu et al. (2024) showed that the radio stars they found by crossmatching LOFAR and VLASS to the GCNS are consistently overluminous in the radio (or under-luminous in the X-ray) compared to the previous Güdel-Benz relation. Callingham et al. (2021) similarly found that the M dwarfs they observed with LOFAR could be orders of magnitude over-luminous in the radio when compared to the canonical Güdel-Benz relation. This is because low-frequency radio emission from stars at is more likely to be coherent radio emission (Bastian 1990), which is more luminous and is not expected to contribute to heating the corona (which contributes to the X-ray emission). Fig. 7 is further evidence of this. However, Vedantham et al. (2022) and Yiu et al. (2024) found a population of chromospherically active, coherent radio emitting stars that follow the relation. It is unclear why these stars adhere to the Güdel-Benz relation at lower frequencies.

The original Güdel–Benz relation was demonstrated using radio detections of stars at 5 and 9 GHz and X-ray detections with *ROSAT*. The eROSITA energy band is similar to the *ROSAT* energy band, but the SRSC currently only includes radio detections below 3 GHz, with most detections from ASKAP between 800 and 1 700 MHz. In future work, we plan to explore the dependence of the Güdel–Benz relation on frequency and whether there are different correlations for different stellar types at different frequencies, or if there is a de-coupling of the relation at lower frequencies. Simultaneous or quasi-simultaneous observations at a wide range of radio frequencies will show if there is a spectral change between 3 and 5 GHz that would indicate a change in the radio mechanism from coherent radio emission to incoherent gyrosynchrotron.

4.3 Comparison with other radio star catalogues

The Catalogue of Radio Stars (CRS; Wendker 1978, 1987, 1995) was constructed by performing literature reviews and included both radio detections and non-detections of stars. In some cases, radio stars were included when a radio source was detected in a dense cluster of stars. In most other cases it included radio stars that were found in targeted searches for stellar radio emission. In this work, we have chosen to include radio detections of stars found in large scale searches for radio stars using SKA precursor and pathfinder instruments and a variety of different methods. This means that the current version of the SRSC will be missing some of the stars in the CRS, including some well known radio stars like BY Draconis and P Cygni.

We have not incorporated the CRS directly into the SRSC because of the inconsistent methods of detection and the challenge of determining the reliability of some of the radio star associations. We plan to evaluate the reliability of detections in the CRS and incorporate them, as part of future work.

We can, however, compare the number of stars in the CRS to the number of stars in the SRSC. The CRS (Wendker 1978, 1987, 1995) contains 1 042 stars detected at frequencies below 420.0 GHz, 228 of which were detected at frequencies below 3 GHz. The SRSC only contains stars detected at frequencies below 3 GHz. We show a histogram of the number of stars detected at various frequencies in the CRS and SRSC in Fig. 8. 127 SRSC stars are in the CRS, 70 of which were detected below 3 GHz in the CRS.

Other searches for radio stars include Becker et al. (2001) and Kimball et al. (2009). Becker et al. (2001) used a 1 arcsec radius to cross-match between FIRST radio sources and optical sources from the Cambridge Automated Plate Measuring Machine scans of the POSS I plates. They classified sources as 'stellar' if the optical source was unresolved and estimated that 98% of the associations they found were physically associated. They found 107 stellar and unknown sources. Kimball et al. (2009) used a 1 arcsec radius to cross-match between FIRST radio sources and Sloan Digital Sky Survey (SDSS; Abazajian et al. 2009) sources. They found 112 matches, but concluded that most of their matches were chance coincidence after filtering and visual inspection. As both of these searches used FIRST data, they only include sources above -10° declination. Although 286 sources in the SRSC are above -10° declination, we do not find any matches between the SRSC and the sources found by Becker et al. (2001) and Kimball et al. (2009). The majority of stars in the SRSC were found via cross-matching (see Fig. 3), and none of the stars from Becker et al. (2001) or Kimball et al. (2009) are in the optical catalogues (see Table 2) we

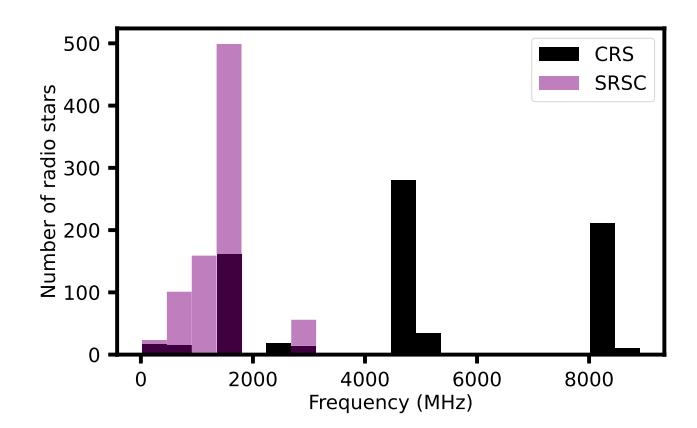


Figure 8. Histogram of the detection frequency of radio stars in the CRS and SRSC. We have only showed the CRS stars detected below 10 GHz here (766 stars). Each star is only counted once. For the CRS stars we include the lowest frequency detection of each star. For the SRSC stars we include the highest frequency detection of each star. We chose to show the frequencies detected this way to demonstrate that even showing the closest set of frequencies, the SRSC contains many more lower frequency detections than the CRS.

cross-matched to. Only 44 of the stars in the SRSC found using the circular polarisation search method (and not via cross-matching) have a Declination $>-10^\circ$. These low numbers mean that it is not surprising that we did not find any sources that were found by Becker et al. (2001) and Kimball et al. (2009). Future searches for radio stars using the VLA and LOFAR, for example, may reveal whether any of the Becker et al. (2001) and Kimball et al. (2009) radio star identifications are reliable.

4.4 Future work

We aim to continue to update the SRSC as more radio stars are identified. To that end, we plan to search for radio detections of eROSITA-identified X-ray emitting stars Freund et al. 2024), VAST-identified variable stars, and more.

As discussed in Section 2.4, we also plan to perform a detailed literature review to include past identifications of radio stars. Please email the corresponding author if you wish to submit radio stars to the SRSC.

The SRSC, particularly as it is expanded and updated in the lead up to the SKA, will be an important resource for identifying radio stars for SKA investigation as well as for predicting the expected population of radio stars, and identifying properties of stellar radio emission so new radio stars can be identified. The SRSC will also be useful for cosmological applications which would benefit from the removal of Galactic foreground sources, for example cosmic microwave background dipole studies (e.g. Siewert, Schmidt-Rubart, & Schwarz 2021; Wagenveld, Klöckner, & Schwarz 2023).

5. Summary

We have presented the SRSC, a catalogue of 839 radio stars identified using circular polarisation searches, cross-matching (with 98% reliability), variability searches, and proper motion searches. This version of the SRSC includes stars found using SKA precursor instruments, and we plan to update the catalogue to include past and future identifications of radio stars. We have demonstrated the science potential of the SRSC using the CMD, radio light curves of a small sample of radio stars and the Güdel–Benz relation.

Acknowledgements. The authors would like to thank Tin Lai for his work on the radio stars catalogue website. LND would like to thank Courtney Crawford, May Gade Pedersen, and Tim Bedding for helpful discussions about Hertzsprung-Russell and colour-magnitude diagrams.

DK is supported by NSF grant AST-1816492.

BJSP acknowledges the traditional owners of the land on which the University of Queensland is situated, upon whose unceded, sovereign, ancestral lands he works, and pays respect to their Ancestors and descendants, who continue cultural and spiritual connections to Country.

LND would like to acknowledge the Gadigal People of the Eora nation, the traditional owners of the land on which most of this work was completed.

KR thanks the LSST-DA Data Science Fellowship Program, which is funded by LSST-DA, the Brinson Foundation, and the Moore Foundation; their participation in the program has benefited this work.

This scientific work uses data obtained from Inyarrimanha Ilgari Bundara/the CSIRO's Murchison Radio-astronomy Observatory. We acknowledge the Wajarri Yamaji People as the Traditional Owners and native title holders of the Observatory site. CSIRO's ASKAP radio telescope is part of the Australia Telescope National Facility. Operation of ASKAP is funded by the Australian Government with support from the National Collaborative Research Infrastructure Strategy. ASKAP uses the resources of the Pawsey Supercomputing Research Centre. Establishment of ASKAP, Inyarrimanha Ilgari Bundara, the CSIRO Murchison Radio-astronomy Observatory, and the Pawsey Supercomputing Research Centre are initiatives of the Australian Government, with support from the Government of Western Australia and the Science and Industry Endowment Fund.

This paper includes archived data obtained through the CSIRO ASKAP Science Data Archive, CASDA.g

This work has made use of data from the European Space Agency (ESA) mission *Gaia*, processed by the *Gaia* Data Processing and Analysis Consortium (DPAC). Funding for the DPAC has been provided by national institutions, in particular the institutions participating in the *Gaia* Multilateral Agreement.

This work uses data from eROSITA, the soft X-ray instrument aboard SRG, a joint Russian-German science mission supported by the Russian Space Agency (Roskosmos), in the interests of the Russian Academy of Sciences represented by its Space Research Institute (IKI), and the Deutsches Zentrum für Luft- und Raumfahrt (DLR). The SRG spacecraft was built by Lavochkin Association (NPOL) and its subcontractors, and is operated by NPOL with support from the Max Planck Institute for Extraterrestrial Physics (MPE). The development and construction of the eROSITA X-ray instrument was led by MPE, with contributions from the Dr. Karl Remeis Observatory Bamberg & ECAP (FAU Erlangen-Nürnberg), the University of Hamburg Observatory, the Leibniz Institute for Astrophysics Potsdam (AIP), and the Institute for Astronomy and Astrophysics of Universität Tübingen, with the support of DLR and the Max Planck Society. The Argelander Institute for Astronomy of the University of Bonn and the Ludwig Maximilians Universität München also participated in the science preparation for eROSITA. The eROSITA data shown here were processed using the eSASS software system developed by the German eROSITA consortium.

This research made use of Astropy, a community-developed core Python package for astronomy (Astropy Collaboration et al. 2013, 2018); and APLpy, an open-source plotting package for Python (Robitaille & Bressert 2012).

This research has made use of the VizieR catalogue access tool (Ochsenbein, Bauer, & Marcout 2000) and the SIMBAD Database (Wenger et al. 2000b), both operated at the CDS, Strasbourg, France.

This publication made use of data products from the Two Micron All Sky Survey, which is a joint project of the University of Massachusetts and the Infrared Processing and Analysis Center/California Institute of Technology, funded by the National Aeronautics and Space Administration and the National Science Foundation.

We would like to thank the referee for their thoughtful and constructive feedback.

ghttp://data.csiro.au/http://data.csiro.au/.

Data availability statement. The Sydney Radio Star Catalogue is available on Vizierh or at https://radiostars.org/. ASKAP data are available in the CSIRO ASKAP Science Data Archive (CASDA). The eROSITA-DE Data Release 1 is available in Vizier (Merloni et al. 2024).j

References

```
Abazajian, K. N., et al. 2009, ApJS, 182, 543
Abbott, D. C., Beiging, J. H., Churchwell, E., & Torres, A. V. 1986, ApJ,
   303, 239
Andersson, A., et al. 2022, MNRAS, 513, 3482
ASTROPY Collaboration, et al. 2013, A&A, 558, A33
ASTROPY Collaboration, et al. 2018, AJ, 156, 123
Babusiaux, C., et al. 2023, A&A, 674 A32
Bailer-Jones, C. A. L., Rybizki, J., Fouesneau, M., Demleitner, M., & Andrae, R.
   2021, AJ, 161, 147
Barrett, P., Dieck, C., Beasley, A. J., Mason, P. A., & Singh, K. P. 2020, ASR,
   66, 1226
Bastian, T. S. 1990, SoPh, 130, 265
Bastian, T. S., Cotton, W. D., & Hallinan, G. 2022, ApJ, 935, 99
Becker, R. H., White, R. L., & Helfand, D. J. 1994, in Astronomical Society of
   the Pacific Conference Series, Vol. 61, Astronomical Data Analysis Software
   and Systems III, ed. D. R. Crabtree, R. J. Hanisch, & J. Barnes, 165
Becker, R. H., White, R. L., & Helfand, D. J. 1995, ApJ, 450, 559
Becker, R. H., et al. 2001, ApJS, 135, 227
Benaglia, P., et al. 2015, A&A, 579 A99
Berger, E., et al. 2001, Natur, 410, 338
Berger, E., et al. 2009, ApJ, 695, 310
Bernardini, F., et al. 2013, MNRAS, 435, 2822
Biswas, A., et al. 2023, MNRAS, 523, 5155
Blomme, R., De Becker, M., Runacres, M. C., van Loo, S., & Setia Gunawan, D.
   Y. A. 2007, A&A, 464, 701
Callingham, J. R., et al. 2019a, NatAs, 3, 82
Callingham, J. R., Vedantham, H. K., Pope, B. J. S., Shimwell, T. W., & LoTSS
   Team. 2019b, RNAAS, 3, 37
Callingham, J. R., et al. 2021, NatAs, 5, 1233
Callingham, J. R., et al. 2023, A&A, 670, A124
Camilo, F., et al. 2018, ApJ, 856, 180
Climent, J. B., Guirado, J. C., Pérez-Torres, M., Marcaide, J. M., & Peña-
   Moñino, L. 2023, Sci, 381, 1120
Crosley, M. K., & Osten, R. A. 2018, ApJ, 856, 39
Das, B., Chandra, P., &Wade, G. A. 2020, MNRAS, 499, 702
Dougherty, S. M., Beasley, A. J., Claussen, M. J., Zauderer, B. A., & Bolingbroke,
   N. J. 2005, ApJ, 623, 447
Dougherty, S. M., &Williams, P. M. 2000, MNRAS, 319, 1005
Driessen, L. N., et al. 2023, PASA, 40, e036
Driessen, L. N., et al. 2022, MNRAS, 510, 1083
Driessen, L. N., et al. 2020, MNRAS, 491, 560
Duchesne, S. W., et al. 2023, PASA, 40, e034
Dulk, G. A. 1985, ARA&A, 23, 169
Duncan, R. A., & White, S. M. 2002, MNRAS, 330, 63
Fabricius, C., et al. 2021, A&A, 649, A5
Fekel, F. C. 1996, AJ, 112, 269
Fender, R., et al. 2016, in MeerKAT Science: On the Pathway to the SKA, 13
Flesch, E. W. 2023, OJA, 6, 49
Freund, S., Czesla, S., Robrade, J., Schneider, P. C., & Schmitt, J. H. M. M. 2022,
   A&A, 664, A105
Freund, S., Robrade, J., Schneider, P. C., & Schmitt, J. H. M. M. 2018, A&A,
   614, A125
Freund, S., et al. 2024, A&A, 684, A121
```

```
GAIA Collaboration, et al. 2016a, A&A, 595, A2
GAIA Collaboration, et al. 2016b, A&A, 595, A1
GAIA Collaboration, et al. 2018, A&A, 616, A1
GAIA Collaboration, et al. 2021a, A&A, 649, A1
GAIA Collaboration, et al. 2021b, A&A, 649, A6
GAIA Collaboration, et al. 2023, A&A, 674, A1
Golovin, A., et al. 2023, A&A, 670, A19
Gordon, Y. A., et al. 2021, ApJS, 255, 30
Güdel, M. 2002, ARA&A, 40, 217
Güdel, M., & Benz, A. O. 1993, ApJ, 405, L63
Guns, S., et al. 2021, ApJ, 916, 98
Haisch, B. M., et al. 1978, ApJ, 225, L35
Hale, C. L., et al. 2021, PASA, 38, e058
Helfand, D. J., Schnee, S., Becker, R. H., White, R. L., & McMahon, R. G. 1999,
   AI, 117, 1568
Hewish, A., Bell, S. J., Pilkington, J. D. H., Scott, P. F., & Collins, R. A. 1968,
   Natur, 217, 709
Hindson, L., et al. 2012, MNRAS, 421, 3418
Høg, E., et al. 2000a, A&A, 357, 367
Høg, E., et al. 2000b, A&A, 355, L27
Hotan, A. W., et al. 2021, PASA, 38, e009
Jones, D. H., et al. 2009, MNRAS, 399, 683
Jones, H., et al. 2005, in Astronomical Society of the Pacific Conference Series,
   Vol. 329, Nearby Large-Scale Structures and the Zone of Avoidance, ed. A.
   P. Fairall, & P. A.Woudt, 11
Kao, M. M., et al. 2016, ApJ, 818, 24
Kao, M. M., Hallinan, G., Pineda, J. S., Stevenson, D., & Burgasser, A. 2018,
   ApJS, 237, 25
Kao, M. M., Mioduszewski, A. J., Villadsen, J., & Shkolnik, E. L. 2023, Natur,
  619, 272
Kawai, H., et al. 2022, PASJ, 74, 477
Kimball, A. E., et al. 2009, ApJ, 701, 535
Lacy, M., et al. 2020, PASP, 132, 035001
Lenc, E., Murphy, T., Lynch, C. R., Kaplan, D. L., & Zhang, S. N. 2018, MNRAS,
   478, 2835
Lovell, B., Whipple, F. L., & Solomon, L. H. 1963, Natur, 198, 228
Lynch, C., Mutel, R. L., & Güdel, M. 2015, ApJ, 802, 106
Masetti, N., et al. 2010, A&A, 519, A96
Matthews, L. D. 2019, PASP, 131, 016001
McConnell, D., et al. 2020, PASA, 37, e048
Merloni, A., et al. 2024, A&A, 682, A34
Murphy, T., et al. 2013, PASA, 30, e006
Murphy, T., et al. 2021, PASA, 38, e054
Ochsenbein, F., Bauer, P., & Marcout, J. 2000, A&AS, 143, 23
O'Sullivan, S. P., McClure-Gri_ths, N. M., Feain, I. J., Gaensler, B. M., & Sault,
   R. J. 2013, MNRAS, 435, 311
Pedersen, M. G., et al. 2019, ApJ, 872, L9
Perley, R. A., Chandler, C. J., Butler, B. J., & Wrobel, J. M. 2011, ApJ, 739, L1
Perryman, M. A. C., et al. 1997, A&A, 323, L49
Predehl, P., et al. 2021, A&A, 647, A1
Pritchard, J., et al. 2024, MNRAS, 529, 1258
Pritchard, J., et al. 2021, MNRAS, 502, 5438
Robitaille, T., & Bressert, E. 2012, APLpy: Astronomical Plotting Library in
   Python, Astrophysics Source Code Library, ascl:1208.017
Rodet, L., et al. 2018, A&A, 618, A23
Rosslowe, C. K., & Crowther, P. A. 2015, MNRAS, 447, 2322
Route, M., &Wolszczan, A. 2012, ApJ, 747, L22
Saikia, D. J., & Salter, C. J. 1988, ARA&A, 26, 93
Samus', N. N., Kazarovets, E. V., Durlevich, O. V., Kireeva, N. N., &
   Pastukhova, E. N. 2017, ARep, 61, 80
Saxton, R. D., et al. 2008, A&A, 480, 611
Seaquist, E. R. 1976, ApJ, 203, L35
Shimwell, T. W., et al. 2017, A&A, 598, A104
Shimwell, T. W., et al. 2022, A&A, 659, A1
Shiohira, Y., et al. 2024, MNRAS, 528, 2136
```

Siewert, T. M., Schmidt-Rubart, M., & Schwarz, D. J. 2021, A&A, 653, A9

Skrutskie, M. F., et al. 2006, AJ, 131, 1163

^hAvailable at CDS via anonymous ftp to cdsarc.u-strasbg.fr (130.79.128.5) or via https://url.au.m.mimecastprotect.com/s/PjB4CzvkyVC8LWjqxI4iLF_?domain=cdsarc.cds.

ihttps://research.csiro.au/casda/https://research.csiro.au/casda/.

jhttps://cdsarc.cds.unistra.fr/viz-bin/cat/J/A+A/682/A34.

Slee, O. B. 1963, Natur, 199, 991 Stein, Y., et al. 2021, A&A, 655, A17 Suresh, A., Chatterjee, S., Cordes, J. M., Bastian, T. S., & Hallinan, G. 2020, ApJ, Tandoi, C., et al. 2024, arXiv e-prints, arXiv:2401.13525 Tingay, S., et al. 2012, in Resolving The Sky - Radio Interferometry: Past, Present and Future, 36 Toet, S. E. B., et al. 2021, A&A, 654, A21 Tovmassian, G., et al. 2017, A&A, 608, A36 van Haarlem, M. P., et al. 2013, A&A, 556, doi: 10.1051/0004-6361/201220873 Vedantham, H. K., et al. 2022, ApJ, 926, L30 Vedantham, H. K., et al. 2020, NatAs, 4, 577 Vidotto, A. A., et al. 2012, MNRAS, 423, 3285 Villadsen, J., & Hallinan, G. 2019, ApJ, 871, 214 Voges, W., et al. 1999, A&A, 349, 389 Wagenveld, J. D., Klöckner, H. R., & Schwarz, D. J. 2023, A&A, 675, A72 Walter, H. G., Hering, R., & de Vegt, C. 1997, A&AS, 122, 529

Wang, Y., et al. 2023, MNRAS, 523, 5661 Wendker, H. J. 1978, AAHam, 10, 3 Wendker, H. J. 1987, A&AS, 69, 87 Wendker, H. J. 1995, A&AS, 109, 177 Wenger, M., et al. 2000a, A&AS, 143, 9 Wenger, M., et al. 2000b, A&AS, 143, 9 Whitehorn, N., et al. 2016, ApJ, 830, 143 Whiting, M., & Humphreys, B. 2012, PASA, 29, 371 Whiting, M. T. 2012, MNRAS, 421, 3242 Williams, P. K. G., & Berger, E. 2015, ApJ, 808, 189 Williams, P. K. G., Cook, B. A., & Berger, E. 2014, ApJ, 785, 9 Wright, E. L., et al. 2010, AJ, 140, 1868 Yiu, T. W. H., Vedantham, H. K., Callingham, J. R., & Günther, M. N. 2024, A&A, 684, A3 Zacharias, N., et al. 2013, AJ, 145, 44 Zic, A., et al. 2020, ApJ, 905, 23

Appendix A. stars table and radio table excerpts

Table A1. The first ten rows of the Stars.dat table. As the Stars.dat table has many columns, we have split the columns and added a 'row' column to include each continuous row.

| conti | nuous row. | | | | | |
|-------|------------|------------------------------|------------------------------|------------------------------|-------------------------|------------------|
| Row | Identifier | Simbad | Gaia | Tycho | 2MASS | GCVS |
| 1 | SRSC 00000 | CPD-62 4126 | Gaia DR3 5853502492753436416 | TYC 9010-2749-1 | 2MASS J14270430-6246553 | |
| 2 | SRSC 00001 | SCR J2241-6119A | Gaia DR3 6406967509044836096 | | 2MASS J22414436-6119311 | |
| 3 | SRSC 00002 | CD-30 6530 | Gaia DR3 5640708647248169600 | TYC 7136-2264-1 | 2MASS J08355977-3042306 | |
| 4 | SRSC 00003 | CD-49 451 | Gaia DR3 4917782741272766592 | TYC 8043-814-1 | 2MASS J01372081-4911443 | |
| 5 | SRSC 00004 | ATO J183.5330+47.2673 | Gaia DR3 1545247048904161664 | | 2MASS J12140814+4716038 | |
| 6 | SRSC 00005 | 2MASS J11414215-6521298 | Gaia DR3 5236539580341818624 | | 2MASS J11414215-6521298 | |
| 7 | SRSC 00006 | Gaia DR3 6090676737160646528 | Gaia DR3 6090676737160646528 | | | |
| 8 | SRSC 00007 | UCAC4 053-023945 | Gaia DR3 6349781084650820608 | | 2MASS J21072847-7926274 | |
| 9 | SRSC 00008 | PM J09551-0819 | Gaia DR3 3771533721761978496 | TYC 5475-507-1 | 2MASS J09550963-0819259 | |
| 10 | SRSC 00009 | Gaia DR3 5971238129102004992 | Gaia DR3 5971238129102004992 | | | |
| Row | HIP | UCAC4 | Survey | Survey_id | Epoch | RAdeg |
| 1 | | UCAC4 137-115021 | GaiaDR3 | Gaia DR3 5853502492753436416 | J2016 | 216.767919155244 |
| 2 | | UCAC4 144-211738 | GaiaDR3 | Gaia DR3 6406967509044836096 | J2016 | 340.436272395047 |
| 3 | | UCAC4 297-048519 | GaiaDR3 | Gaia DR3 5640708647248169600 | J2016 | 128.998712548091 |
| 4 | HIP 7554 | UCAC4 205-001600 | GaiaDR3 | Gaia DR3 4917782741272766592 | J2016 | 24.34012397651 |
| 5 | | UCAC4 687-053931 | GaiaDR3 | Gaia DR3 1545247048904161664 | J2016 | 183.532979271787 |
| 6 | | UCAC4 124-048667 | GaiaDR3 | Gaia DR3 5236539580341818624 | J2016 | 175.425221260026 |
| 7 | | | GaiaDR3 | Gaia DR3 6090676737160646528 | J2016 | 211.790382522137 |
| 8 | | UCAC4 053-023945 | GaiaDR3 | Gaia DR3 6349781084650820608 | J2016 | 316.869374569023 |
| 9 | | UCAC4 409-049725 | GaiaDR3 | Gaia DR3 3771533721761978496 | J2016 | 148.789425163571 |
| 10 | | | GaiaDR3 | Gaia DR3 5971238129102004992 | J2016 | 253.074412168032 |
| Row | e_RAdeg | DEdeg | e_DEdeg | plx | e_plx | pmRA |
| 1 | 6e-06 | -62.782098179545 | 9e-06 | 1.53 | 0.01 | -3.841 |
| 2 | 8e-06 | -61.325706059717 | 1e-05 | 35.2 | 0.01 | 150.4 |
| 3 | 8e-06 | -30.70858670455 | 1e-05 | 15.7 | 0.01 | -64.11 |
| 4 | 1e-05 | -49.195143947004 | 1e-05 | 45.12 | 0.01 | 496.1 |
| 5 | 1e-05 | 47.267364915243 | 1e-05 | 25.76 | 0.02 | -137.2 |
| 6 | 1e-05 | -65.358320600806 | 1e-05 | 9.92 | 0.02 | -40.18 |
| 7 | 1e-05 | -50.034311567705 | 1e-05 | 10.99 | 0.02 | -54.59 |
| 8 | 1e-05 | -79.441225054251 | 1e-05 | 14.44 | 0.02 | 28.66 |
| 9 | 1e-05 | -8.323892037812 | 1e-05 | 31.53 | 0.02 | -135.68 |
| 10 | 2e-05 | -38.189228568212 | 1e-05 | 6.08 | 0.02 | -11.18 |
| Row | e_pmRA | pmDE | e_pmDE | Radio_multiple | Identification_method | |
| 1 | 0.007 | -5.44 | 0.01 | 0.0 | 18 | |
| 2 | 0.01 | -87.89 | 0.01 | 0.0 | 18 | |
| 3 | 0.01 | -14.3 | 0.01 | 0.0 | 18 | |
| 4 | 0.01 | 116.1 | 0.01 | 0.0 | 18 | |
| 5 | 0.01 | -72.58 | 0.01 | 0.0 | 16 | |
| 6 | 0.02 | -4.38 | 0.02 | 0.0 | 18 | |
| 7 | 0.02 | -46.85 | 0.02 | 0.0 | 16 | |
| 8 | 0.02 | -61.04 | 0.02 | 0.0 | 16 | |
| 9 | 0.02 | -7.06 | 0.02 | 0.0 | 18 | |
| 10 | 0.02 | -22.68 | 0.02 | 0.0 | 16 | |
| | | | | | | |

Table A2. The first ten rows of the Radio.dat table. As the Radio.dat table has many columns, we have split the columns and added a 'row' column to include each continuous row.

| Row | Identifier | Match_separation | Radio_id | Field | Obs_date | Exposure | RAdeg | DEdeg | e_RAdeg | e_DEdeg |
|-----|------------|------------------|-------------------------|----------|---------------------|-----------|-----------|-----------|-----------------------|---------|
| 1 | SRSC 00000 | 1.2 | SB50301_component_4182a | 50 301.0 | 2023-06-02T12:53:55 | 716.0 | 216.7685 | -62.7823 | 2.0 | 2.0 |
| 2 | SRSC 00000 | | SB47240_component_3629a | 47 240.0 | 2023-01-20T21:45:43 | 726.0 | 216.7677 | -62.783 | | |
| 3 | SRSC 00000 | 1.7 | SB51817_component_4823a | 51 817.0 | 2023-08-03T08:56:08 | 727.0 | 216.7675 | -62.7817 | 2.0 | 2.0 |
| 4 | SRSC 00000 | 1.6 | SB45665_component_4457a | 45 665.0 | 2022-11-19T01:13:36 | 717.0 | 216.767 | -62.7823 | 2.0 | 2.0 |
| 5 | SRSC 00000 | 0.7 | SB45667_component_4705a | 45 667.0 | 2022-11-19T01:40:28 | 717.0 | 216.7676 | -62.7823 | 2.0 | 2.0 |
| 6 | SRSC 00000 | 0.7 | SB45821_component_4152b | 45 821.0 | 2022-11-24T23:41:57 | 36011.0 | 216.7681 | -62.7819 | 2.0 | 2.0 |
| 7 | SRSC 00000 | 2.5 | SB51522_component_4617a | 51 522.0 | 2023-07-21T10:00:19 | 726.0 | 216.7664 | -62.782 | 2.0 | 2.0 |
| 8 | SRSC 00000 | 2.1 | SB53482_component_4650a | 53 482.0 | 2023-10-04T03:45:51 | 737.0 | 216.7689 | -62.7817 | 2.0 | 2.0 |
| 9 | SRSC 00000 | 1.1 | SB22350_component_2094a | 22 350.0 | 2021-02-01T20:56:05 | 895.0 | 216.7673 | -62.7821 | 2.0 | 2.0 |
| 10 | SRSC 00000 | 2.2 | SB47236_component_4433a | 47 236.0 | 2023-01-20T20:45:20 | 726.0 | 216.7684 | -62.7827 | 2.0 | 2.0 |
| Row | Freq | Speakl | e_Speakl | Stotl | e_Stotl | bmax | bmin | PA | e_bmax | e_bmin |
| 1 | 887.5 | 1.6 | 0.3 | 1.5 | 0.5 | 17.0 | 11.0 | 123.01 | 3.0 | 2.0 |
| 2 | 887.5 | 2.1 | 0.2 | 2.8 | 0.4 | | | | | |
| 3 | 887.5 | 1.2 | 0.2 | 1.5 | 0.3 | 18.0 | 13.0 | 22.94 | 2.0 | 2.0 |
| 4 | 887.5 | 1.6 | 0.2 | 1.8 | 0.3 | 19.0 | 11.0 | 134.44 | 2.0 | 1.0 |
| 5 | 887.5 | 1.4 | 0.2 | 1.7 | 0.4 | 16.0 | 15.0 | 86.21 | 2.0 | 2.0 |
| 6 | 943.5 | 0.64 | 0.03 | 0.74 | 0.05 | 17.5 | 15.0 | 133.57 | 0.7 | 0.7 |
| 7 | 887.5 | 1.4 | 0.2 | 1.6 | 0.4 | 22.0 | 10.0 | 141.85 | 2.0 | 2.0 |
| 8 | 887.5 | 1.3 | 0.2 | 1.4 | 0.4 | 17.0 | 13.0 | 133.59 | 3.0 | 2.0 |
| 9 | 1 367.5 | 1.6 | 0.3 | 1.6 | 0.5 | 9.0 | 8.0 | 170.91 | 2.0 | 1.0 |
| 10 | 887.5 | 1.4 | 0.2 | 1.7 | 0.4 | 20.0 | 11.0 | 135.82 | 2.0 | 2.0 |
| Row | Survey | SpeakV | e_SpeakV | StotV | e_StotV | Telescope | localrmsV | localrmsI | Ref | |
| 1 | | | | | | ASKAP | | 0.26 | ThisWork | |
| 2 | VAST 23e | 1.3 | | 1.9 | | ASKAP | | 0.29 | 10.1093/mnras/stab299 | |
| 3 | | | | | | ASKAP | | 0.22 | ThisWork | |
| 4 | | | | | | ASKAP | | 0.21 | ThisWork | |
| 5 | | | | | | ASKAP | | 0.24 | ThisWork | |
| 6 | 10-11hour | | | | | ASKAP | | 0.03 | ThisWork | |
| 7 | | | | | | ASKAP | | 0.25 | ThisWork | |
| 8 | | | | | | ASKAP | | 0.24 | ThisWork | |
| 9 | | | | | | ASKAP | | 0.28 | ThisWork | |
| 10 | | | | | | ASKAP | | 0.24 | ThisWork | |